JGR Oceans

RESEARCH ARTICLE
10.1029/2021JC018087

Special Section:
Uncovering the hidden links between dynamics, chemical, biogeochemical and biological processes under the changing Arctic

A Refinement of the Processes Controlling Dissolved Copper and Nickel Biogeochemistry: Insights From the Pan-Arctic

Laramie T. Jensen[1,2], Jay T. Cullen[3], Sarah L. Jackson[3,4], Loes J. A. Gerringa[5], Dorothea Bauch[6,7], Rob Middag[5], Robert M. Sherrell[8,9], and Jessica N. Fitzsimmons[1]

[1]Department of Oceanography, Texas A&M University, College Station, TX, USA, [2]Cooperative Institute for Climate, Ocean, and Ecosystem Studies, University of Washington, Seattle, WA, USA, [3]School of Earth and Ocean Sciences, University of Victoria, Victoria, BC, Canada, [4]Research School of Earth Sciences, The Australian National University, Canberra, ACT, Australia, [5]Department of Ocean Systems, Royal Netherlands Institute for Sea Research (NIOZ), Texel, The Netherlands, [6]Leibniz Laboratory for Radiometric Dating and Stable Isotope Research, Kiel University, Kiel, Germany, [7]GEOMAR Helmholtz Centre for Ocean Research, Kiel, Germany, [8]Department of Marine and Coastal Sciences, Rutgers University, New Brunswick, NJ, USA, [9]Department of Earth and Planetary Sciences, Rutgers University, New Brunswick, NJ, USA

Abstract Recent studies, including many from the GEOTRACES program, have expanded our knowledge of trace metals in the Arctic Ocean, an isolated ocean dominated by continental shelf and riverine inputs. Here, we report a unique, pan-Arctic linear relationship between dissolved copper (Cu) and nickel (Ni) present north of 60°N that is absent in other oceans. The correlation is driven primarily by high Cu and Ni concentrations in the low salinity, river-influenced surface Arctic and low, homogeneous concentrations in Arctic deep waters, opposing their typical global distributions. Rivers are a major source of both metals, which is most evident within the central Arctic's Transpolar Drift. Local decoupling of the linear Cu-Ni relationship along the Chukchi Shelf and within the Canada Basin upper halocline reveals that Ni is additionally modified by biological cycling and shelf sediment processes, while Cu is mostly sourced from riverine inputs and influenced by mixing. This observation highlights differences in their chemistries: Cu is more prone to complexation with organic ligands, stabilizing its riverine source fluxes into the Arctic, while Ni is more labile and is dominated by biological processes. Within the Canadian Arctic Archipelago, an important source of Arctic water to the Atlantic Ocean, contributions of Cu and Ni from meteoric waters and the halocline are attenuated during transit to the Atlantic. Additionally, Cu and Ni in deep waters diminish with age due to isolation from surface sources, with higher concentrations in the younger Eastern Arctic basins and lower concentrations in the older Western Arctic basins.

Plain Language Summary The trace metals copper and nickel are key elements involved in the biological and chemical cycles present in the ocean that help fuel the algae forming the base of the marine food web. The Arctic Ocean is heavily influenced by inputs from land including river discharge and continental sediments, and it has limited exchange with other oceans. We found that dissolved copper and nickel have Arctic distributions unique from the rest of the global ocean and are also surprisingly linearly correlated in the Arctic. We carefully compared them to each other and to other chemical tracers in order to identify the processes that control their distributions. We found that copper and nickel concentrations are highest in Western Arctic surface waters, due to riverine discharge for both metals, and also continental shelf sources of nickel. In deeper waters, copper and nickel concentrations are low and constant, unlike in other ocean basins. Also, unique to the Arctic, biological cycling was not a controlling factor for copper and nickel behavior, and interactions of these metals with particles were also less than observed elsewhere. Overall, the Arctic was an ideal case study for the importance of different ocean processes on controlling marine copper and nickel.

Key Points:

- Dissolved Cu and Ni share a unique linear correlation in the Arctic Ocean, with high surface water and low deep water concentrations
- Cu is sourced primarily from rivers, while Ni is also sourced from sediments on the Chukchi Shelf
- Concentrations of both are lower in Western than in Eastern Arctic deep waters, and both are attenuated in the Canadian Arctic Archipelago

Supporting Information:

Supporting Information may be found in the online version of this article.

Correspondence to:

J. N. Fitzsimmons,
jessfitz@tamu.edu

Citation:

Jensen, L. T., Cullen, J. T., Jackson, S. L., Gerringa, L. J. A., Bauch, D., Middag, R., et al. (2022). A refinement of the processes controlling dissolved copper and nickel biogeochemistry: Insights from the pan-Arctic. *Journal of Geophysical Research: Oceans*, *127*, e2021JC018087. https://doi.org/10.1029/2021JC018087

Received 2 OCT 2021
Accepted 18 APR 2022

Author Contributions:

Conceptualization: Jay T. Cullen, Loes J. A. Gerringa, Robert M. Sherrell, Jessica N. Fitzsimmons
Data curation: Laramie T. Jensen, Jay T. Cullen, Sarah L. Jackson, Loes J. A. Gerringa, Dorothea Bauch, Rob Middag, Jessica N. Fitzsimmons
Formal analysis: Laramie T. Jensen, Sarah L. Jackson, Dorothea Bauch, Rob Middag

1. Introduction

Trace metals serve as essential micronutrients for marine phytoplankton as well as tracers of important biogeochemical processes. Nickel (Ni) is classified as a "nutrient-type" element based on its macronutrient-like profile shape. Nutrient-type elemental cycling is relatively simple compared to copper (Cu), for example, which is a "hybrid-type" element because it often has a distinct, linearly increasing concentration trend with depth, indicating that abiotic processes also play a role in controlling its distribution, in conjunction with biological cycling

Funding acquisition: Jay T. Cullen, Loes J. A. Gerringa, Robert M. Sherrell, Jessica N. Fitzsimmons
Investigation: Laramie T. Jensen, Loes J. A. Gerringa, Dorothea Bauch, Rob Middag, Jessica N. Fitzsimmons
Methodology: Laramie T. Jensen, Jay T. Cullen, Loes J. A. Gerringa, Rob Middag, Jessica N. Fitzsimmons
Project Administration: Jessica N. Fitzsimmons
Resources: Jay T. Cullen, Loes J. A. Gerringa, Dorothea Bauch, Rob Middag, Robert M. Sherrell, Jessica N. Fitzsimmons
Supervision: Jay T. Cullen, Loes J. A. Gerringa, Jessica N. Fitzsimmons
Validation: Laramie T. Jensen, Loes J. A. Gerringa, Rob Middag, Robert M. Sherrell
Visualization: Laramie T. Jensen
Writing – original draft: Laramie T. Jensen, Jessica N. Fitzsimmons
Writing – review & editing: Laramie T. Jensen, Jay T. Cullen, Sarah L. Jackson, Loes J. A. Gerringa, Dorothea Bauch, Rob Middag, Robert M. Sherrell, Jessica N. Fitzsimmons

(Bruland et al., 2014). Copper serves as an essential metalloenzyme center for proteins such as cytochrome oxidase (Wood, 1978), iron acquisition proteins (Maldonado et al., 2006), and denitrification proteins (Granger & Ward, 2003), and at low oceanic Cu concentrations, Cu even has the potential to co-limit primary production alongside other micronutrients (Annett et al., 2008). However, high concentrations of available Cu are toxic to phytoplankton (Moffett et al., 1997), which can be mitigated by surface complexation of Cu by organic ligands (>95%, Coale & Bruland, 1988; Moffett & Brand, 1996) that buffer labile Cu concentrations at non-toxic levels more conducive to phytoplankton growth (Bruland et al., 2014).

Scavenging onto particles facilitates Cu removal from deep waters (Boyle et al., 1977; Moore, 1978; Noriki et al., 1998), explaining why its concentration does not increase as much as the nutrient-type metals along the deep water flow path of thermohaline circulation. However, copper's profile increases linearly with depth, suggesting a sediment/deep water source (Biller & Bruland, 2013; Hines et al., 1984) and/or reversible scavenging at depth, similar to thorium (Bacon & Anderson, 1982). Margin and benthic sources have been proposed as significant inputs of Cu to both surface and bottom waters (Boyle et al., 1981; Heggie et al., 1987), pointing to the important role of sediments alongside rivers and aerosol fluxes, which are the major external sources of Cu to the global ocean (Richon & Tagliabue, 2019).

Nickel also serves as an essential micronutrient and has a "macronutrient-like" profile shape with surface depletion and regeneration at depth, although it is not fully depleted at the surface (Middag et al., 2020; Schlitzer et al., 2018). As a protein metal center, it catalyzes the assimilation of urea in the enzyme urease and serves as the center of the nickel superoxide dismutase enzyme (Broering et al., 2013; Dupont et al., 2008; Sunda, 2012; Twining & Baines, 2013). Nickel has been found to be co-limiting with nitrogen under laboratory conditions (Price & Morel, 1991) and is implicated in the limitation of nitrogen fixation (Ho, 2013), which is of particular interest in areas like the Arctic Ocean that are nitrogen limited (Rijkenberg et al., 2018; Taylor et al., 2013). While Ni speciation has been studied much less than metals such as iron and Cu, 10%–60% of Ni has been reported to be bound by organic ligands (Donat et al., 1994; Saito et al., 2004; Vraspir & Butler, 2009). Unlike some other nutrient-type metals, Ni appears to have both shallow and deep water regeneration, similar to phosphate and silicate, respectively (Böning et al., 2015; Sclater et al., 1976), which perhaps points to the important role of diatom activity in controlling Ni's global distribution and relationship to macronutrients (Böning et al., 2015; Middag et al., 2020; Twining & Baines, 2013). Beyond biological uptake and regeneration, the inputs of Ni to the ocean are not well constrained, although continental margin and river sources have been suggested to play a significant role (Bowie et al., 2002; Cameron & Vance, 2014; Little et al., 2020; Westerlund et al., 1986).

Because of their different profile shapes and biogeochemical controls, Cu and Ni are not often directly compared in oceanographic investigations. Some early studies of trace metals established global baselines of multiple trace metal distributions and so did compare Cu and Ni alongside other nutrient-type elements such as cadmium (Cd) and Zn (Boyle et al., 1981; Bruland, 1980; Danielsson et al., 1985; Dickson & Hunter, 1981; Nolting & de Baar, 1994; Noriki et al., 1998; Spivack et al., 1983; Yeats et al., 1995), but these studies rarely juxtaposed Cu and Ni directly. Notably, Cu and Ni have both been observed to be complexed by coastal organic matter (Abualhaija et al., 2015; Gerringa et al., 1991; Whitby & van den Berg, 2015) and, as divalent metals, may compete for similar ligand groups in the open ocean (Boiteau et al., 2016). A comparison of the two could provide insight into the relative importance of biological and physicochemical processes in shaping their respective distributions, as both share riverine and continental sources (Böning et al., 2015; Richon & Tagliabue, 2019) and some nutrient-like dynamics.

The Arctic Ocean is a unique ocean basin in which to study trace metal cycling because it is more dominated by continental shelf area (>50%, Jakobsson et al., 2004) and riverine fluxes (Ekwurzel et al., 2001) than any other ocean basin. Additionally, the Arctic Ocean is a point of mixing between the North Atlantic and North Pacific Oceans, which have starkly different trace metal signatures (Gerringa et al., 2021; Sunda, 2012). Prior studies of trace metals in the Arctic have noted high Cu, Ni, and other trace metal concentrations in surface and subsurface waters (Cid et al., 2012; Gerringa et al., 2021; Jensen et al., 2019; Klunder, Bauch, et al., 2012; Klunder, Laan, et al., 2012; Kondo et al., 2016; Middag et al., 2011; Moore, 1981; Yeats, 1988; Yeats & Westerlund, 1991). The origin of these subsurface enrichments in the Western Arctic is the Chukchi Shelf and the upper halocline water mass that exports shelf material offshore into the central Arctic (Cid et al., 2012; Jensen et al., 2019; Kondo

et al., 2016), while the surface enrichment is likely due in part to the river-influenced Transpolar Drift (TPD) that bisects the central Arctic (Charette et al., 2020).

Here, we exploit these unique Arctic characteristics to distinguish the processes that control Cu and Ni biogeochemistry in the oceans. We assembled a pan-Arctic Cu and Ni data set from the GEOTRACES GN01 section in the Western Arctic, the GEOTRACES GN04 section in the Eastern Arctic, and the GEOTRACES GN02/03 section in the Canadian Arctic (Figure 1). This data set combines previously published Cu and Ni results from GN04 (Gerringa et al., 2021) and from the central Arctic (>84°N, upper 50 m of GN01 [Charette et al., 2020]) with the full-depth, complete GN01 transect, and unpublished GN02 and GN03 transects. Both Charette et al. (2020) and Gerringa et al. (2021) focused on a synthesis of multiple parameters including trace metals, nutrients, and accompanying isotopes. A pan-Arctic perspective focused solely on Cu and Ni allows us to identify the processes delivering Cu and Ni to the Arctic and diagnose why their distribution in the Arctic is so different than that in other major ocean basins.

2. Methods

2.1. Sample Collection

A map of all sampling locations for this study is shown in Figure 1. Methods for the previously published dissolved Cu, Ni, nutrient, and oxygen isotope data along GN04 (PS94, 17 August to 14 October 2015) can be found in Gerringa et al. (2021). Seawater samples were collected on the 2015 U.S. Arctic GEOTRACES GN01 cruise aboard the USCGC *Healy* between 9 August and 12 October 2015 and on the 2015 Canadian Arctic GEOTRACES GN02 and GN03 cruises aboard the CCGS *Amundsen* between 10 July and 1 October 2015.

The GN01 Western Arctic cruise originated in the North Pacific (Figure 1, Station 1) and continued through the Bering Strait northward along 170°–180°W across the western Chukchi Shelf to the North Pole ("northbound") and then back southward along 150°W to terminate again on the eastern Chukchi Shelf ("southbound"). Full depth samples were taken within the Bering Strait, Chukchi Shelf, and Canada, Makarov, and Amundsen basins (Figure 1). Additionally, clean near-surface samples were collected from shallow casts (1–20 m) through ice holes at select stations (Stations 31, 33, 39, 42, 43, and 46) north of 84°N and within the marginal ice zone (MIZ).

The GN02 and GN03 cruises cover an area between the Labrador Sea at 56°N, through Baffin Bay and the Canadian Arctic Archipelago (CAA), terminating in the Canada Basin, sampling 17 full depth stations. Designated intercalibration "overlap" stations were GN01 Station 30 and GN04 Station 101 as well as GN01 Station 57 and GN03 Station CB4 (Canada Basin; Figure 1; Figure S1 in Supporting Information S1).

Dissolved trace metals Cu and Ni were collected on GN01 following established trace metal clean GEOTRACES protocols (Cutter et al., 2010; Cutter & Bruland, 2012). Briefly, seawater was collected using a trace metal clean CTD rosette (Sea-Bird Electronics Inc.) on a Vectran cable, equipped with 24 × 12 L Go-Flo bottles. The Go-Flo bottles were tripped at the desired sampling depth on ascent at ∼3 m/min, and upon recovery each bottle was immediately moved into a clean, positive pressure sampling area and pressurized (∼0.5 atm) with HEPA-filtered air. Each Go-Flo bottle was fitted with a 0.2 µm AcroPak-200 polyethersulfone filter capsule (Pall), and seawater was filtered into an acid cleaned 250 mL low-density polyethylene (LDPE) Nalgene bottle following three 10% volume rinses of the bottle, cap, and threads. Samples were promptly acidified to 0.012 M hydrochloric acid (HCl) using 250 µL of Optima grade HCl.

Similar procedures were used along GN02 and GN03 where a trace metal clean CTD (Sea-Bird 911) rosette with 12 L Go-Flo bottles on a Kevlar line was used to collect all samples. Seawater was filtered using the same 0.2 µm AcroPak-200 filter capsules into acid cleaned LDPE (Bel Art) bottles. Samples were then promptly acidified to 0.012 M HCl (Baseline, SeaStar Chemicals).

2.2. Analysis

Following nine months storage, GN01 samples were pre-concentrated for dissolved Cu and Ni using a SeaFAST-pico system (ESI, Omaha, NE, USA) at Texas A&M University, coupled with an isotope dilution and stand-

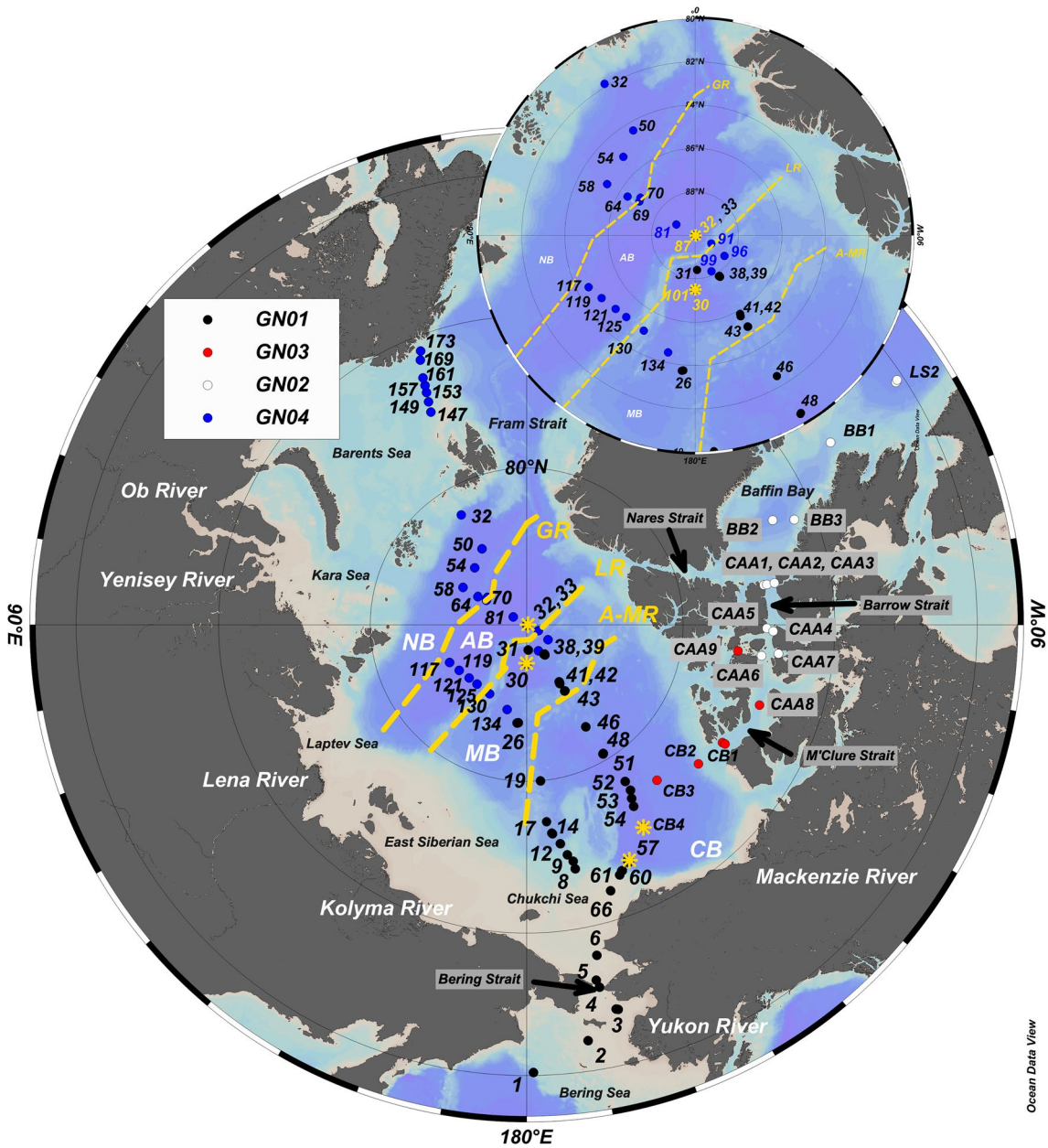

Figure 1. GEOTRACES Arctic GN01, GN01, GN03, and GN04 transect labeled with relevant stations, rivers, seas, and bathymetric features identified. Black dots refer to GN01, red dots GN03, white dots GN02, blue dots GN04. AB, Amundsen Basin, MB, Makarov Basin, CB, Canada Basin, LR, Lomonosov Ridge, A-MR, Alpha-Mendeleev Ridge, GR, Gakkel Ridge. An inset is included to show the detail above 85°N. The yellow asterisks refer to overlap/intercalibration stations (see Figure S1 in Supporting Information S1).

ard curve method following Lagerström et al. (2013) and fully described in Jensen, Wyatt, et al. (2020). A 10 mL aliquot of sample was taken up by the SeaFAST system following equilibration with ^{65}Cu and ^{62}Ni spike, subsequently buffered on-line to pH 6.2 ± 0.3, and immediately loaded onto a column containing Nobias-chelate PA1 resin. The bound metals were then back-eluted with 10% (v/v) HNO_3 (Optima, Fisher Scientific) into a 400 µL aliquot (25x preconcentration). This eluent was then analyzed promptly in medium resolution on a Thermo Element XR high-resolution inductively coupled plasma mass spectrometer (HR-ICP-MS) at the R. Ken Williams Radiogenic laboratory at Texas A&M University.

Table 1
Precision and Accuracy of Dissolved Metal Measurements

	GN01			GN02/03*			GN04**			Consensus value	
	Element (nmol/kg)			Element (nmol/kg)			Element (nmol/kg)			Element (nmol/kg)	
CRM	*n*	Ni	Cu	*n*	Ni	Cu	*n*	Ni	Cu	Ni	Cu
SAFe D1	35	8.609	2.035	14	8.64	2.15	6	8.54	1.990	8.580	2.270
stdev		0.176	0.081		0.30	0.09		0.084	0.020	0.260	0.110
SAFe D2	32	8.714	2.192							8.630	2.280
stdev		0.166	0.099							0.250	0.150
SAFe S	4	2.401	0.544	14	2.31	0.49				2.280	0.520
stdev		0.020	0.013		0.09	0.05				0.090	0.050
	Element (pmol/kg)			Element (pmol/kg)			Element (pmol/kg)				
	n	Ni	Cu	*n*	Ni	Cu	*n*	Ni	Cu		
Average blank	31	15.2	12.4	10	53	30	24	7.4	8.2		
Std deviation of blank	29	2.82	1.69	10	10	2.7	24	4.00	10.70		
Detection limit	29	8.45	5.08	10	30	8	24	12.00	32.10		

Note. Standard reference materials such as SAFe D1 were used by all labs to assess the accuracy of their measurements, with labs reporting an average and a standard deviation based on *n* replicates. All labs were in good agreement with the consensus values. Blanks and detection limits (defined as 3 x standard deviation of the blank) are reported in the bottom half of the table. *originally reported in Jackson (2017) and ** Gerringa et al. (2021).

Analysis of the GN02 and GN03 samples was carried out according to methodology established in Jackson et al. (2018). Samples were analyzed in a Class-100 clean room at the University of Victoria, British Columbia. Trace-metal extraction and preconcentration was performed using the seaFAST-pico system (ESI). The automated seaFAST system preconcentrated samples while removing the bulk seawater matrix through solid phase extraction (Lagerström et al., 2013). For each sample, 20 mL of seawater was loaded onto a Nobias-chelate PA1 resin column. The column was then rinsed with an ammonium acetate buffer solution (pH = 6.0), which was prepared by bubbling high-purity anhydrous ammonia gas through twice-distilled acetic acid with the pH adjusted by additions of NH_3 to remove the matrix. Samples were back-eluted with 10% (v/v) HNO_3 (Baseline, SeaStar Chemicals, Sidney, BC, Canada) into a 2.5 mL aliquot (8x preconcentration). The preconcentrated samples were subsequently analyzed using an Agilent 8800 ICP-MS/MS.

The results from the intercalibration exercise among these four cruises show significant and strong agreement between laboratories and analysis methods for both dissolved Cu and Ni across all depths, indicating that data from all three labs can be compared directly with confidence (Figure S1 in Supporting Information S1). Accuracy, precision, procedural blanks, and limits of detection of these measurements are summarized in Table 1.

2.3. Hydrographic and Nutrient Analyses

Salinity, silicate, and other macronutrients collected along GN01 were determined shipboard by the Scripps Institute of Oceanography Ocean Data Facility (SIO ODF) team. Parameters such as temperature and pressure were taken directly from the trace metal CTD (Sea-Bird 911+) sensors. Bottle salinity from trace metal Go-Flo bottles was measured using a Guildline Autosal 8400B salinometer. Dissolved macronutrients phosphate, and silicate were analyzed on a SEAL Analytical AutoAnalyzer 3 (Hydes et al., 2010).

Along GN02 and GN03, macronutrient samples were collected directly from the rosette and analyzed shipboard on a Bran + Luebbe AutoAnalyzer 3 following methods adapted from Grasshoff et al. (2009).

2.4. Oxygen Isotope Analyses and Fractional Water Mass Analysis

This study uses previously reported oxygen isotope data and fractional water mass analyses from GN01 (Charette et al., 2020; Newton et al., 2013) and GN04 (PO* method, Bauch et al., 2011; Gerringa et al., 2021). Along GN02/GN03, oxygen isotopic composition of freshwater was determined following the CO_2 equilibration method of Epstein and Mayeda (1953), and freshwater endmember determination for a fractional water mass analysis utilized data for practical salinity, total alkalinity, and dissolved inorganic carbon from Eicken et al. (2002), Miller et al. (2011), Rysgaard et al. (2007) and Yamamoto-Kawai et al. (2009).

Note that endmembers and analyses differed among the various transects but yielded good comparison for the fractions of sea ice melt and meteoric water.

3. Hydrographic Context

The Arctic Ocean is an isolated basin, dominated by shallow continental shelves and limited in exchange with the Pacific and Atlantic Oceans via narrow and relatively shallow sills (50 and 620 m, respectively). In addition, the Arctic has year-round ice coverage, and it receives 11% of the global riverine flux despite composing only 1% of the ocean by volume (Opsahl et al., 1999). This leads to a large freshwater reservoir in Arctic surface waters. Subsurface water masses are dictated largely by changes in salinity, due to brine rejection during sea ice formation and the relatively isothermal nature of polar oceans.

Arctic surface waters, also known as the polar mixed layer (PML), extend approximately 0–50 m (Rudels, 2015; Talley et al., 2011). In the Western Arctic (Canada and Makarov basins, Figure 1), the PML mainly comprises Pacific waters advected through the Bering Strait (50 m sill), riverine discharge, and ice melt, and along the GN01 transect it has a low salinity of 22–31 and a potential temperature ranging −1.8°C to 1.8°C. Within the Eastern Arctic (Nansen and Amundsen basins, Figure 1), the PML is saltier due to more Atlantic water influence (Rudels, 2015). This layer is well ventilated and well-mixed, but its low salinity establishes strong stratification from denser water below. A prominent feature of the PML is the surface TPD that brings Eastern Arctic shelf-modified river water across the central Arctic Ocean and out through the Fram Strait and Canadian Archipelago (Rudels, 2015). The TPD is characterized by (terrigenous) organic matter and trace metals (Charette et al., 2020) and affects GN01 Stations 30–43 and GN04 Stations 81–101, 119–130 (Gerringa et al., 2021). For the purposes of this study, we consider the PML to extend from the surface to the sharp salinity increase, indicating the first subsurface water mass: the halocline.

The cold halocline of the Western Arctic Ocean is a unique feature formed on Arctic continental shelves as a result of brine rejection during sea ice formation (Aagaard et al., 1981). The Canada Basin of the Western Arctic presents with a "double" halocline, due to the presence of advected Pacific waters over the Chukchi Shelf. As brine is rejected during sea ice formation on the shallow Chukchi Shelf, a cold, salty water mass forms and subducts under the PML and extends well into the Canada basin, forming the Upper Halocline Layer (UHL, S 31–33.1, ∼50–150 m; Aagaard et al., 1981; Shimada et al., 2005; Woodgate et al., 2005). Often, the UHL is delineated by its elevated silicate (Si) > 25 μmol/kg (Anderson et al., 2013; Jones & Anderson, 1986; Figure S2 in Supporting Information S1). Below this, there is a Lower Halocline Layer (LHL, S 33.1–34.7, ∼150–300 m), which originates from Atlantic-derived shelf waters mixed with UHL waters (Jones & Anderson, 1986). In contrast, the Makarov basin has a "single" halocline (S 31.0–34.3, ∼50–100 m) that is primarily derived from the Eurasian (Eastern Arctic) shelves mixed with some Pacific-derived waters (Rudels, 2015). Likewise, the Amundsen Basin has a single, Eurasian-influenced halocline (S 32.7–34.7; Rudels et al., 2004). In the Nansen Basin (present along GN04), the halocline is formed from the advection of Atlantic water across the shelves and through the St. Anna trough, cooling and freshening such that it is situated between the PML and underlying Atlantic waters (Coachman & Barnes, 1963; Rudels, 2015).

Below the halocline, the warm intermediate Atlantic waters dominate across the entire Arctic Ocean. These layers are important because Eastern Arctic intermediate and deep waters exchange with the Nordic Seas through the Fram Strait (2,600 m sill depth) and the North Atlantic via the Greenland-Scotland Ridge (620 m sill depth). The Arctic's upper Atlantic layer (AL), called the Fram Strait Branch (FSB, ∼350–800 m, Rudels et al., 2004), has a noticeable maximum in potential temperature of $\theta > 0$°C. Below this, there is another Atlantic-derived layer known as the Barents Sea Branch, which includes waters mixed from the shallower Barents Sea (Schauer

et al., 2002; Woodgate et al., 2001). Below the ALs are the homogenous, Arctic deep waters: Canada Basin Deep Water ($S > 34.92$, $-0.55°C < \theta < -0.5°C$) and Eurasian Basin Deep Water ($34.92 < S < 34.95$, $\theta < -0.7°C$; Aagaard et al., 1985; Talley et al., 2011).

The CAA and Baffin Bay, sampled along GEOTRACES sections GN02 and GN03 (Figure 1), represent an important outflow of Arctic waters to the North Atlantic. Pacific and Atlantic-origin waters circulate eastward within the Canada Basin, become entrained into the Beaufort Gyre (BG, GN01 Stations 48–60 and GN03 Stations CB1-4) and other cyclonic surface currents, and ultimately enter the CAA. Shallow sills at the M'Clure Strait (375 m) and Barrow Strait (125 m) prevent deep water intrusion into the CAA, but the UHL nutrient maximum that is characteristic of the Canada Basin can also be found throughout the CAA and into Baffin Bay. These upper ocean waters mix with Arctic outflow from the Nares Strait and eventually transit southward toward the Labrador Sea and North Atlantic.

4. Results and Discussion

4.1. Copper and Nickel in the Arctic Ocean

The major result of this study is that dissolved Cu and Ni share a remarkably similar distribution across the pan-Arctic (Figures 2 and 3) that results in their strong linear correlation (dCu = [0.841±0.01]*dNi – 1.35±0.05, $r^2 = 0.87$, $p < 0.01$, where the uncertainty is reported as standard error in the regression, Figure 4b). This similarity between dissolved Ni and Cu distributions is unique to the Arctic and contrasts with the distributions of these elements in other major ocean basins in four important ways. First, Arctic Cu reaches higher concentrations than found in other major ocean basins (Figure 4a). Second, Arctic profile shapes of Cu and Ni are unique and do not follow the strict "hybrid-type" and "nutrient-type" profile shapes, respectively, that are observed in the rest of the global ocean (Figure S3 in Supporting Information S1); we note that the Western Arctic also has unique profile shapes of Zn (Jensen et al., 2019), Cd (Zhang et al., 2019), Co (Bundy et al., 2020), Fe (Jensen, Morton, et al., 2020), and macronutrients, pointing to the unique properties of the Arctic. Third, Cu and Ni in the Arctic have similar distributions (Figures 2 and 3), leading to their linear correlation (Figure 4b), while instead a nonlinear "kink" is found in the Cu-Ni relationship of other ocean basins (Figure 4a). Finally, both Cu and Ni concentrations are very low and homogenous in Arctic deep waters. This final observation may be an important clue in resolving these unique concentration patterns. The high Cu and Ni concentrations driving the linear Cu-Ni relationship come from surface and intermediate waters (upper 500 m, cold colors in Figure 4a), while deeper Arctic waters have low, homogenous concentrations (warm colors in Figure 4a).

To identify the processes responsible for the unique Cu and Ni distributions and correlations in the Arctic Ocean, the following sections will summarize the distribution of Cu and Ni with depth, within each major water mass and geographic area of the Arctic Ocean, comparing Cu and Ni with other chemical tracers that are diagnostic of various source and sink terms in the Arctic.

4.1.1. Surface Distribution of Cu and Ni

Arctic surface concentrations of Ni and Cu were noticeably higher than surface concentrations in the Atlantic and Pacific (Figure 4a and Figure S4 in Supporting Information S1). Average surface concentrations and standard deviations (±1 SD) across all four transects in the upper 20 m are shown in Table 2. All four Arctic transects synthesized here had significantly higher surface concentrations than the global averages of 0.80 ± 0.64 and 3.18 ± 1.53 nmol/kg reported for surface Cu and Ni, respectively (Schlitzer et al., 2018). Note that average surface concentrations were higher and more variable along GN01 and GN04, where highest concentrations occurred within the TPD (Charette et al., 2020; Gerringa et al., 2021). Additionally, the Cu-Ni relationship was strong in the surface waters 0–20 m depth across all four cruises (dCu = [0.95±0.03]*dNi – 1.53±0.18, $r^2 = 0.88$, $p < 0.01$, Table 2). The correlation between Cu or Ni and salinity (Figure 5) suggests that freshwater inputs are an important source for both metals. What processes are responsible for these uniquely high surface concentrations? We test and evaluate below three hypothesized fluxes: sea ice melt, riverine fluxes, and continental shelf inputs.

4.1.2. Sea Ice Melt in the MIZ

Sea ice melt has the potential to be a large source of trace metals to surface seawater (Aguilar-Islas et al., 2008; Hölemann et al., 1999; Lannuzel et al., 2016; Measures, 1999; Tovar-Sánchez et al., 2010), as sea ice can deliver

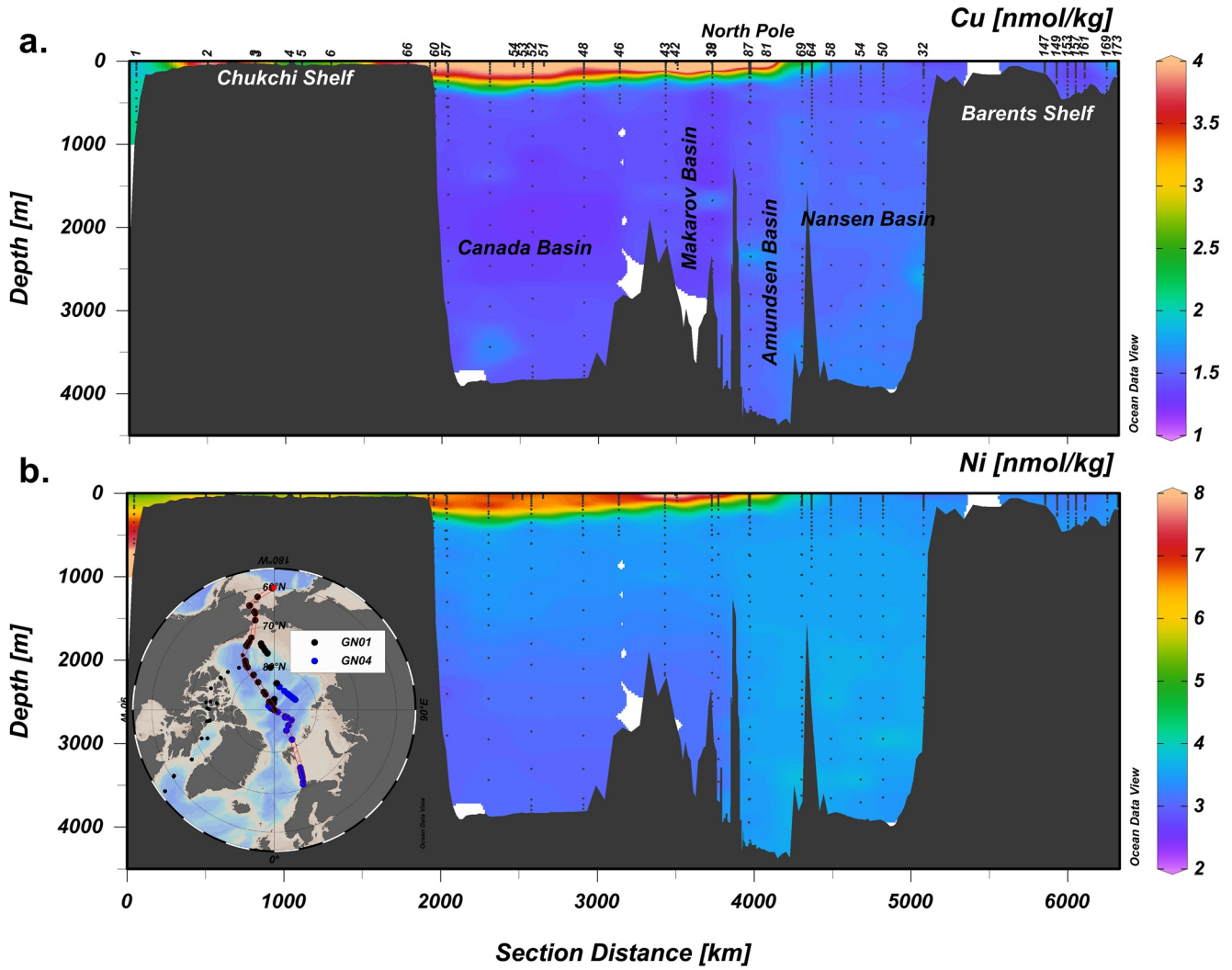

Figure 2. Section plots of (a) Cu and (b) Ni across GN01 and GN04. The section is shown in the inset map beginning in the North Pacific (GN01 Station 1) and ending on the Barents Shelf (GN04 Station 173). Major basins and representative stations are also identified in panel (a). Cu and Ni show a similar distribution across both transects. See Figure S2 in Supporting Information S1 for Si and P sections.

metals and nutrients accumulated in brine channels or carried in ice-rafted sediments (Measures, 1999) from the continental shelves to anywhere in the Arctic where ice is melting (Kadko et al., 2016; Krumpen et al., 2019). Concentrations of Cu and Ni in Arctic sea ice have a wide observed range, from 10.7 to 430 nmol/kg and 1–830 nmol/kg, respectively (Hölemann et al., 1999; Marsay et al., 2018; Tovar-Sánchez et al., 2010), which could thus act as a source or a diluent of surface Arctic seawater dissolved Cu and Ni concentrations upon melting. Notably, the sea ice Cu and Ni concentrations measured on the GN01 cruise were on the very low end, at or below this range (Marsay et al., 2018): 0.67 ± 0.44 nmol/kg for Cu and 0.75 ± 0.47 nmol/kg for Ni. Both are significantly lower than surface Arctic seawater concentrations, hinting that sea ice is unlikely to be the source of the high surface seawater Cu and Ni concentrations observed in this study.

Nonetheless, we employed the tracers $\delta^{18}O_{sw}$ and salinity to obtain the fraction of water contributed by sea ice melt ("f_{sim}") (Newton et al., 2013) at stations designated within the "MIZ" along GN01 (MIZ, Stations 8–17, 51–57), defined as stations where ice was present but coverage was <100%. Nickel had a negative relationship with f_{sim} (Figure 6d, $r^2 = 0.87$, $p < 0.01$, pink dots), indicating that sea ice melt acted as a diluent rather than a source to surface waters. Indeed, the extrapolated sea ice concentration of Ni was indistinguishable from zero (0.18 ± 0.94 nmol/kg), which is within the range quoted above (Marsay et al., 2018). There was no relationship between f_{sim} and Cu, likely due to Stations 8 and 9 over the Chukchi Shelf, which are known to receive shelf

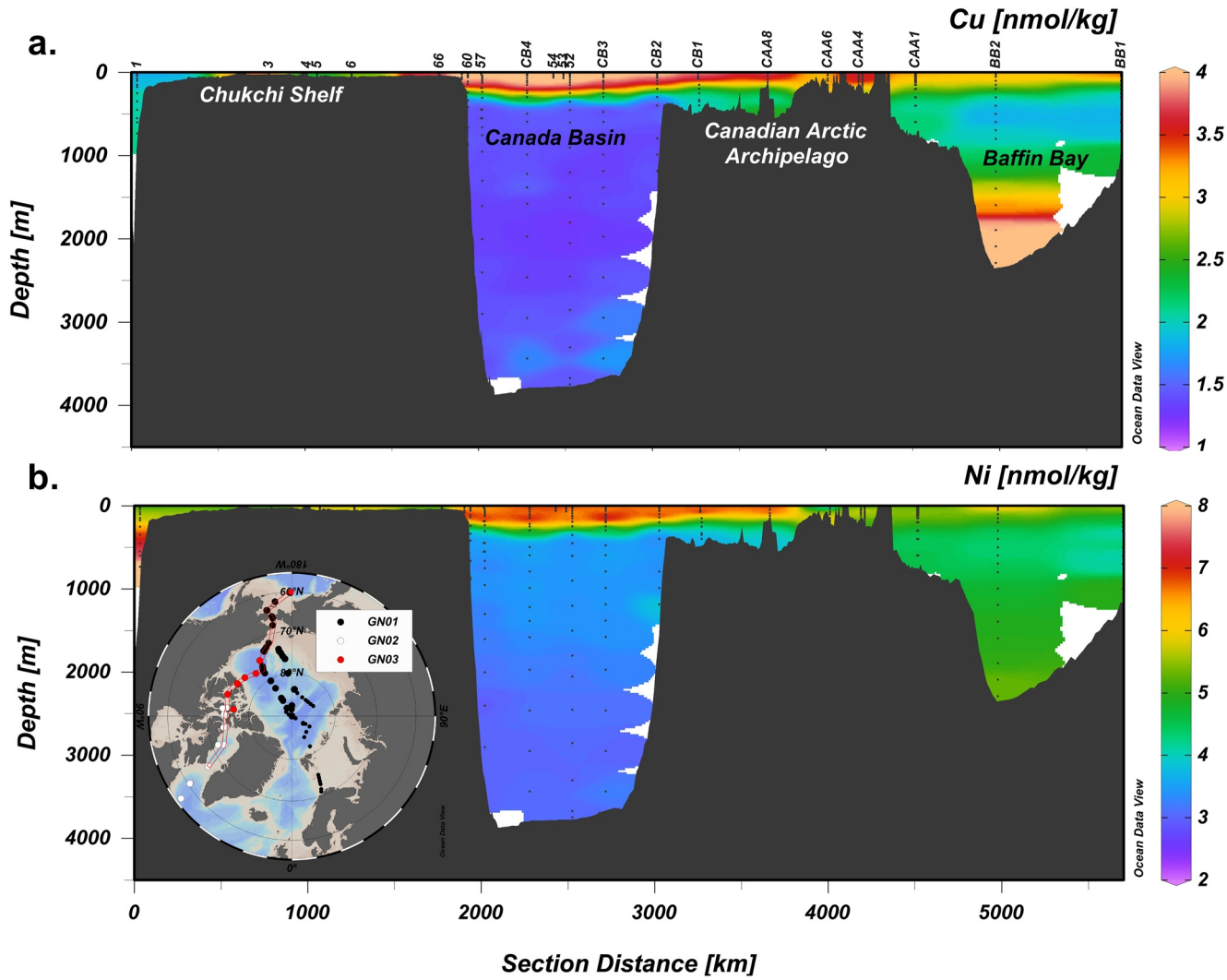

Figure 3. Section plots of (a) Cu and (b) Ni across GN01, GN02, and GN03. The section is shown in the inset map beginning in the North Pacific (GN01 Station 1) and ending in Baffin Bay (GN02 Station BB1). Major basins and representative stations are also identified in panel (a). Dissolved Cu and Ni show a similar distribution across both transects. See Figure S2 in Supporting Information S1 for Si and P sections.

sediment fluxes that could affect the relationship of metals to sea ice melt along this transect (Jensen et al., 2019; Figure 6c, red circles). Along GN03 in the same geographic region, high surface f_{sim} values yielded a positive correlation with Cu ($r^2 = 0.72$, $p < 0.01$, Figure 6c), indicating a sea ice melt source of Cu within the BG. Extrapolation to a 100% f_{sim} value suggests that sea ice in this area may have a Cu concentration of ~9 nmol/kg. For Ni, the relationship with f_{sim} appeared to be absent at these GN03 stations ($r^2 = 0.17$, Figure 6d). Therefore, sea ice melt is not the source of the surface seawater concentration maximum for Ni in the Western Arctic and in fact only serves to dilute these concentrations upon melting, but sea ice may contribute to elevated Cu concentrations near the CAA (Figure 6c). Previously published results from GN04 in the Eastern Arctic show that both Cu and Ni were also negatively correlated to f_{sim}, again indicative of dilution (Gerringa et al., 2021).

4.1.3. Riverine Inputs of Copper and Nickel

The low salinity PML, where dissolved Cu and Ni concentrations were elevated (Figures 2 and 3), is attributed to the large volume of riverine freshwaters carried into the Arctic Ocean. Previous studies used the tracers $\delta^{18}O_{SW}$ and salinity to elucidate the fraction of meteoric water contribution ("f_{met}") in the surface ocean; meteoric water contains contributions from both river water and precipitation (rain or snow). As Charette et al. (2020) have discussed, the TPD carried the highest fractions of meteoric water and thus appeared to drive the correlation with

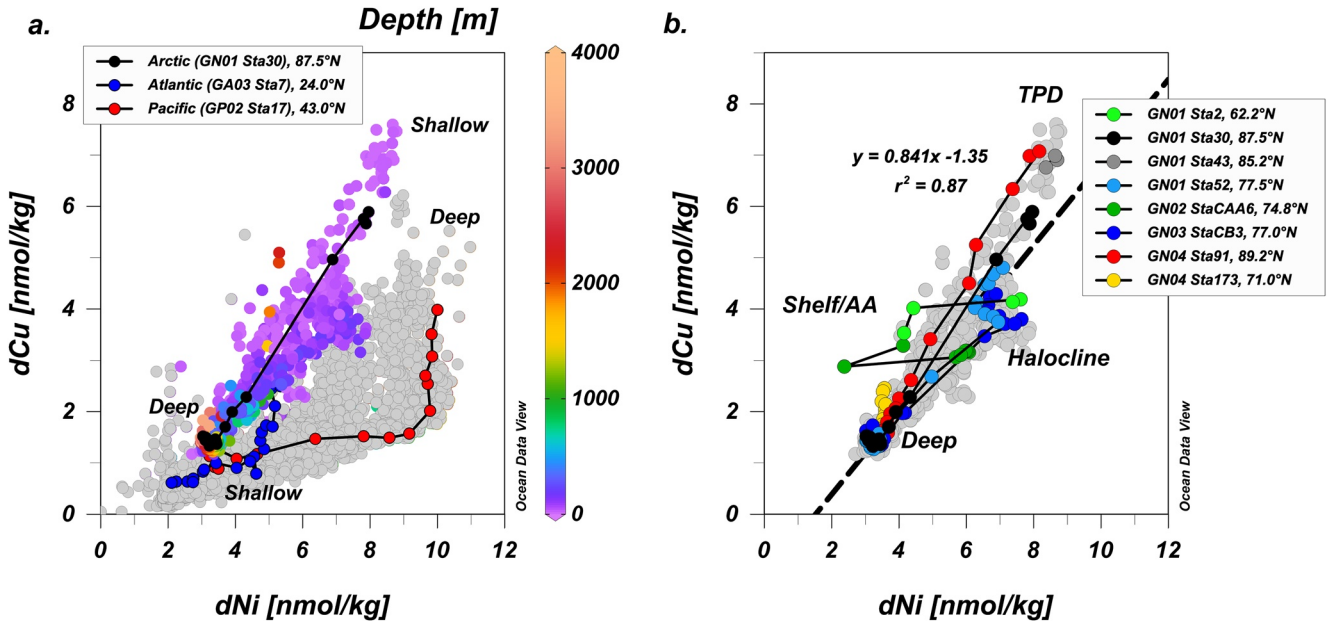

Figure 4. Dissolved Cu vs. Ni concentrations (a) globally (from the GEOTRACES IDP-2017) and (b) within the Arctic Ocean only (GN01-03 and GN04 [Gerringa et al., 2021]). In (a), the global stations are in light gray with two representative Atlantic (blue, GP02) and Pacific (red, GA03) stations highlighted to demonstrate how uniquely linear the Cu-Ni relationship is within the Arctic (colored). Also, surface Arctic concentrations are high, and deep water concentrations are low compared to opposite nutrient-type trends across the rest of the global ocean. In (b), all Arctic data are in light gray, with representative stations indicated by single colors, such as the TPD (red, dark gray, black), the halocline (light and dark blue), the shelves (light and dark green), and the "background" Eastern Arctic (yellow).

f_{met} for both Cu and Ni along GN01 and GN04 (Figures 6a and 6b, $r^2 = 0.92, 0.83$, $p < 0.01$, respectively). The TPD receives freshwater from multiple rivers along the Siberian shelves, but nevertheless presents a remarkably cohesive relationship among Ni, Cu, and f_{met}, as well as Cu/Ni, in the central Arctic. In fact, when the overall relationship between f_{met} and Cu and Ni is extrapolated to 100% meteoric water, a riverine end-member concentration of 22 nmol/kg for Cu and 23 nmol/kg for Ni is calculated, which is within the range of the currently known Eurasian Arctic river endmembers (~3–38 and ~4–23 nmol/kg, respectively, summarized in Table S1 in Supporting Information S1). Thus, the TPD plays a driving role in the observed surface maxima of Cu and Ni and the pan-Arctic linear relationship between Cu and Ni.

Table 2
Average Surface (0–20 m) Concentrations Across All Four Arctic Cruises (GN01, GN02, GN03, GN04) for Cu and Ni ± Standard Deviation

	Cu (nmol/kg)	Ni (nmol/kg)
GN01 (0–20 m)	4.57 ± 1.50	6.59 ± 1.25
GN02 (0–20 m)	3.17 ± 0.65	4.93 ± 0.83
GN03 (0–20 m)	3.98 ± 0.31	6.37 ± 0.70
GN04 (0–20 m)	3.64 ± 2.09	5.20 ± 2.02
Global (0–20 m)	0.80 ± 0.64	3.18 ± 1.53
Cu/Ni relationship (0–20 m)	dCu = [0.95(±0.03)]*dNi – 1.53(±0.18), $r^2 = 0.88$	
Cu/Ni relationship (all depths)	dCu = [0.841(±0.01)]*dNi – 1.35(±0.05), $r^2 = 0.87$	

Note. The global surface average is taken from Schlitzer et al. (2018). In the bottom half of the table the Cu/Ni linear relationship is reported for the surface and across all four cruises transect throughout all depths. Note that GN01 Station 1 (North Pacific endmember) is excluded from all calculations within this table, as are GN02 stations K1, LS1, and LS2 (North Atlantic/Labrador Sea endmembers).

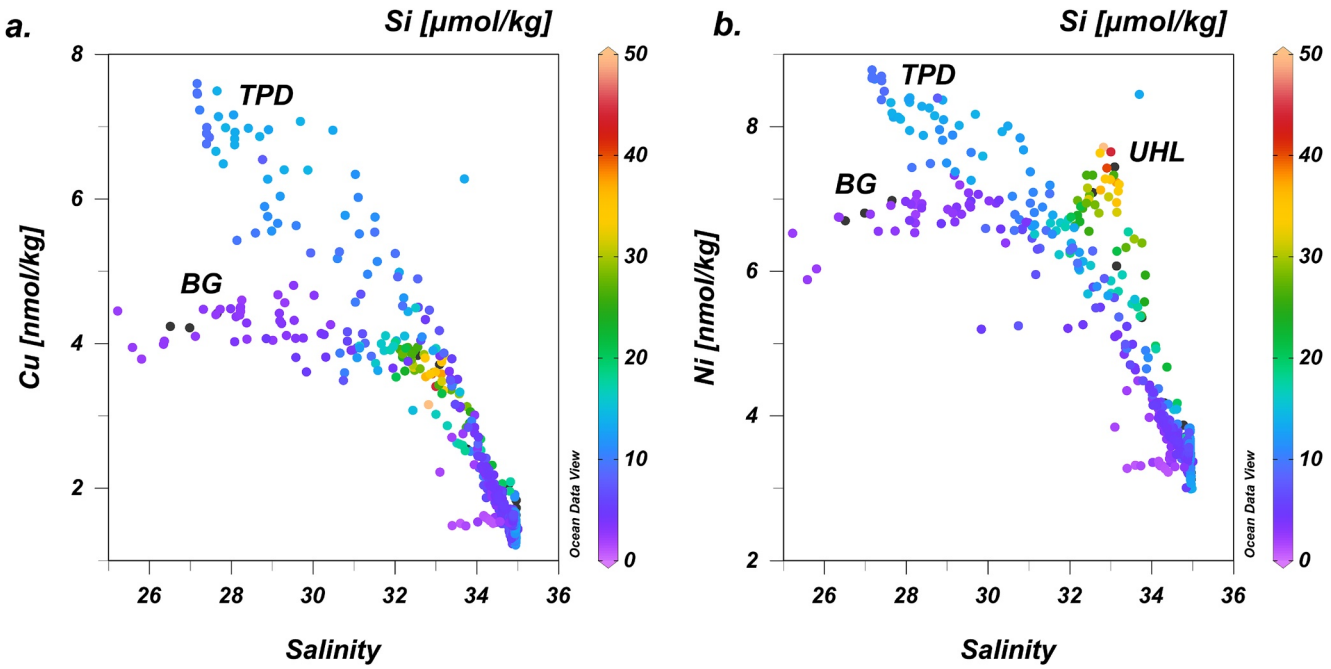

Figure 5. Plots of (a) Cu and (b) Ni vs. salinity across the Arctic basin at all depths (>75°N, GN01-04). Silicate is overlaid in color to indicate the UHL (UHL Si > 25 µmol/kg). Black dots indicate stations where Si concentrations were not available. Note that Ni is particularly elevated in the UHL. Also note that both Cu and Ni have two distinct freshwater (low salinity) metal sources: the TPD (with higher Cu and Ni concentrations) and the Beaufort Gyre (with lower Cu and Ni concentrations). TPD, Transpolar Drift, BG, Beaufort Gyre, UHL, upper halocline layer.

A recent study along the GN04 transect noted that there may be distinct plumes from the Lena River water and Yenisei/Ob River water that can be differentiated using εNd values within the TPD (Paffrath et al., 2021). The less saline, and less radiogenic, Lena River-influenced (~0–30 m) water overlies saltier, more radiogenic, Yenisei/Ob water (~50–100 m). While Cu and Ni vs. f_{met} slopes showed some subtle variation within the TPD water mass, as observed by Gerringa et al. (2021), they were also both negatively correlated to εNd in this study ($r^2 = 0.64$ and 0.58, respectively, $p < 0.01$, Figure S5 in Supporting Information S1). This suggests that the Lena River may contribute slightly higher Cu and Ni compared to the underlying Yenisei/Ob Rivers. However, concentrations in these rivers and estuaries were similar in range and magnitude (Table S1 in Supporting Information S1), and thus the different riverine sources for these dissolved metals could not be distinguished clearly.

In this study, Cu and Ni were also elevated in surface waters outside of the TPD (Figures 6a and 6b). The surficial BG also holds a significant freshwater reservoir (Proshutinsky et al., 2009). Interestingly, although f_{met} was elevated in the BG, there was no significant linear relationship between f_{met} and either Cu or Ni ($r^2 = 0.34$, $r^2 = 0.006$, respectively, Figures 6a and 6b). Although riverine fluxes make up a large component of the BG freshwater inventory, low salinity Pacific-derived waters flowing through the Bering Strait are another important source of freshwaters to the BG (Carmack et al., 2008). The Yukon River outflow is entrained in the northward flowing Alaskan Coastal Waters that tightly hug the western Alaskan coast and contribute to the Canada Basin UHL as well as the BG. This is especially true when atmospheric conditions lead to a negative Arctic Oscillation index and thus allow for a more expansive BG (Steele et al., 2004), as was seen in the years preceding 2015. In fact, the concentrations of Cu and Ni in the BG were similar to those found along the Bering Strait, Chukchi Shelf, and in the UHL (Figure 7), suggesting that Pacific-derived water entrained into the BG may have influenced the concentrations. Scavenging or biological uptake of Cu and Ni could play a role in keeping concentrations uniform, as has been suggested for other geochemical tracers in the same region (Guay et al., 2009). Even at stations close to the CAA where the Mackenzie River outflow is often observed, there was very little meteoric water contribution. Overall, meteoric water did not appear to play a controlling role in the distribution of Cu and Ni within the BG or within water entering the CAA.

The Chukchi Shelf stations had overall low f_{met} and lower concentrations of Cu and Ni (Figures 6a and 6b), despite the known presence of the Yukon River outflow near Stations 2 and 3 (Figure 1). For Ni, the overall Arctic

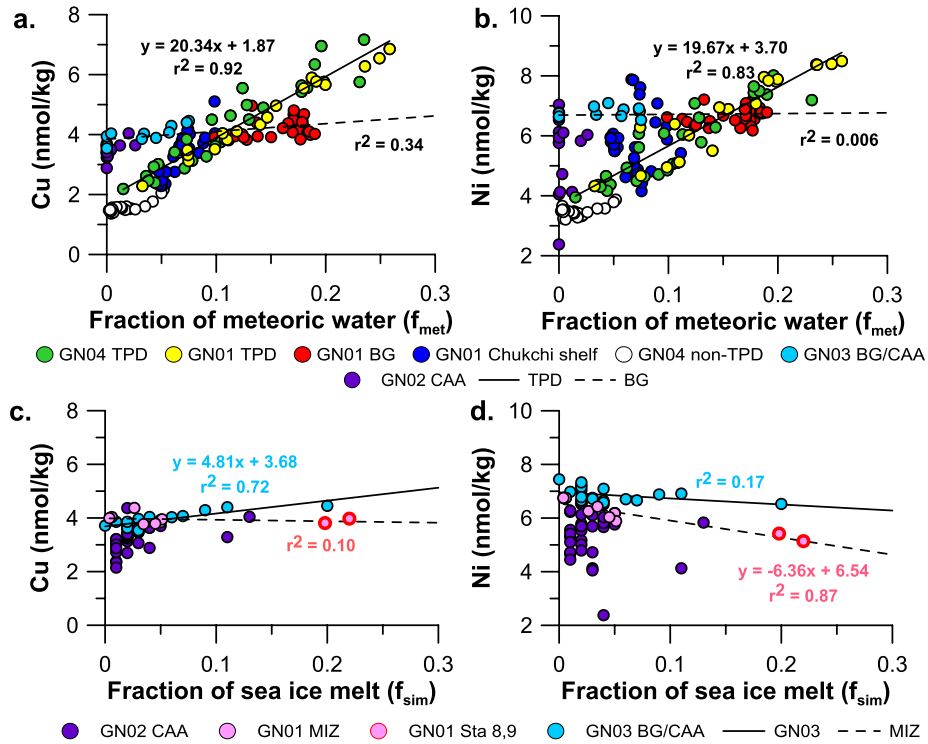

Figure 6. Plots of Cu and Ni vs. fraction of meteoric water (a, b) and fraction of sea ice melt (c, d) in surface waters (<50 m). TPD, Transpolar Drift, BG, Beaufort Gyre, MIZ, marginal ice zone. Various linear relationships are shown in the legend (dashed or solid lines). Colors are used to differentiate major geographic areas such as the shelves, the CAA, and central Arctic. Note that GN04 "non-TPD" include stations 50, 54, 58, 64 outside of the TPD. GN01 Stations 8 and 9 are circled in red in (c, d) to highlight their high f_{sim} values in the MIZ.

f_{met} relationship was driven primarily by the TPD samples (Figure 6), while Ni was not correlated to f_{met} along the Chukchi Shelf (Figure S6b in Supporting Information S1) or within the BG. Copper, in contrast, did display correlations to f_{met} along the Chukchi Shelf (Figure S6a in Supporting Information S1), as well as within the TPD, indicating that riverine fluxes are particularly critical for setting surface Arctic Cu distributions. This is in line with what we know about the role of organic ligands in stabilizing Cu, particularly in estuarine environments (Abualhaija et al., 2015; Laglera & van den Berg, 2003; Whitby & van den Berg, 2015). Previous studies in the Arctic highlight the role of terrestrially derived humic substances entering the Arctic via the TPD as well as other river sources in controlling Fe distribution and speciation (Laglera et al., 2019; Slagter et al., 2017, 2019). Given that up to 69% of dissolved Cu may be bound by these humic substances (Abualhaija et al., 2015), we suggest that river-derived organic matter may be preferentially binding Cu, compared to Ni. Similar ligands bind Ni(II) and Cu(II) in marine and estuarine environments, but Cu(II)-humic complexes are more preferred following the Irving Williams Series (Irving & Williams, 1953), and Cu will outcompete Ni for stronger ligands (Boiteau et al., 2016). Based on these results, Cu appears to be controlled more significantly by riverine fluxes than does Ni, and rivers are likely the dominant driver of the increase in Cu moving from the North Pacific (GN01 Station 1) through the Bering Strait and Chukchi Shelf. Increased phytoplankton uptake of Ni compared to Cu may also account for the decoupling of Ni and Cu in surface waters and is discussed below.

4.1.4. Modifications Across the Chukchi, Barents, and CAA Continental Shelves

The third potential Cu and Ni surface source that we investigated was benthic fluxes from the Bering Strait, Chukchi, CAA, and Barents continental shelves. While Figure 6 provides strong evidence of riverine influence, the Chukchi Shelf and CAA stations showed substantial deviation from the pan-Arctic Cu and Ni linear relationship shown in Figure 4b, as well as the Ni vs. f_{met} relationship in Figure 6b. An examination of the Bering and Chukchi Shelf Cu and Ni distributions during GN01 showed that along the transect, northward from the North Pacific "end member" at Station 1 across the Bering Strait and Chukchi Shelf, both Cu and Ni concentrations increased in surface waters (Figure 7 and Figure S4 in Supporting Information S1). This surface increase was

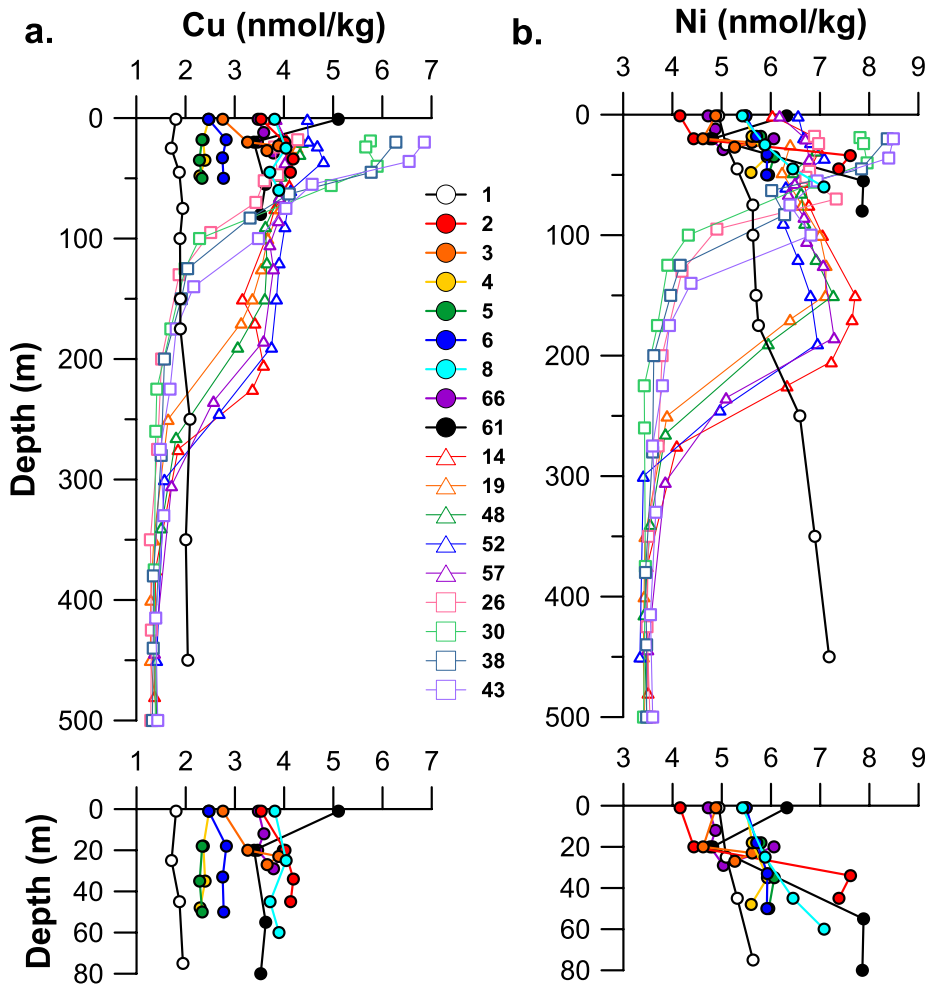

Figure 7. Profile overlay of the concentrations from GN01 of (a) Cu and (b) Ni across the entire transect in the upper 500 m of the water column (Station 32 in Amundsen Basin excluded). A grouping of Bering and Chukchi Shelf stations (Stations 2–8, 61–66, closed circle symbols) demonstrate the change in Cu and Ni in the upper water column moving from Station 1 across the continental shelf. Offshore there are higher Cu and Ni concentrations in the UHL of the Canada Basin (Stations 14, 19, 48–57 open triangle symbols) than in the halocline of the Makarov Basin (Stations 26–43, open square symbols).

most noticeable for Cu, which increased by ~2 nmol/kg from Station 1 (1.84 ± 0.09 nmol/kg) to the Chukchi Shelf break at stations 8 and 61 (3.89 ± 0.53 nmol/kg). Copper concentrations at each of these shelf stations were constant with depth (Figure 7a, inset). Dissolved Ni did not appear to increase as significantly along the shelf from ~5.0 nmol/kg at Pacific Station 1 to 5.5–6.0 nmol/kg at the shelf break (Figure 7b). However, there were two features of the Ni distribution over the shelf that distinguish it from the distribution of Cu. First, Ni did not follow Cu's more successive northward increase. Second, Ni profiles were not constant with depth (Figure 7b, inset) and instead increased significantly toward the bottom, sometimes with gradients of 2–3 nmol/kg Ni between surface and bottom waters over the shelf (Figure 7b). This decoupling over the shelf translated to a breakdown of the otherwise linear Cu-Ni relationship (Figure S6c in Supporting Information S1), despite both elements increasing in concentration relative to Pacific waters, suggesting distinct controlling processes over the shelf.

Copper is traditionally thought to have a benthic source (Boyle et al., 1981; Richon & Tagliabue, 2019), and Ni can be released from sediments during diagenetic remobilization from the reduction of Mn oxide phases and other mineral transformations (Little et al., 2020) or the regeneration of organic matter below the sediment-water interface. Under mildly reducing conditions, dissolved Cu may have a benthic, continental shelf source (Heggie, 1982; Heggie et al., 1987), while under euxinic conditions, Cu precipitates in sediments as an inorganic sulfide (Biller & Bruland, 2013). Previous studies have established that benthic fluxes from the Chukchi Shelf can control trace metal distributions in the rest of the Western Arctic in two distinct ways: elements such as dissolved Fe,

Mn, and Co are supplied by reductive dissolution of Chukchi Shelf sediments (Aguilar-Islas et al., 2013; Bundy et al., 2020; Jensen, Morton, et al., 2020; Kondo et al., 2016; Vieira et al., 2019), while dissolved Zn and the macronutrients are supplied by porewater fluxes of remineralized Zn-rich organic matter (Jensen et al., 2019). A principal component analysis done by Vieira et al. (2019) along the Chukchi Shelf showed a relationship between Ni, Zn, and the macronutrients, while Cu was not strongly correlated to either Ni, the macronutrients, or Fe and Mn. We compare our Cu and Ni data to the distributions of each of these metals along the Chukchi Shelf to elucidate which of these mechanisms might be driving benthic fluxes of Cu and Ni.

Chukchi Shelf sediment porewaters are low in oxygen, creating a reducing environment that remobilizes redox-active metals such as Fe, Mn, and Co (Jensen, Morton, et al., 2020; Vieira et al., 2019). However, Cu did not share a strong correlation with Fe or Mn but did have a reductive, benthic source. Likewise, Cu was not correlated to the major macronutrients along the shelf in this study. In fact, Cu had a significant correlation only to f_{met} along the shelf (Figure 6a and Figure S6a in Supporting Information S1), suggesting that river input may be responsible for the Cu distribution along the Chukchi Shelf.

Dissolved Ni was moderately correlated with Zn along the Strait and Shelf stations ($r^2 = 0.72$, $p < 0.01$, Figure S6d in Supporting Information S1). Like Zn, Ni was also correlated at these sites with the macronutrient silicate (Si, $r^2 = 0.69$, $p < 0.01$, Figure S7e in Supporting Information S1), which is known to be released during the dissolution of diatoms in sediments along the Chukchi Shelf alongside Zn (Jensen et al., 2019), suggesting that the Ni flux from sediments was also driven by regeneration of exported phytoplankton detritus. This is consistent with a greater Ni demand of diatoms compared to other phytoplankton groups (Twining et al., 2012), which might produce a Zn and Ni flux from Chukchi Shelf sediments following regeneration in porewaters or at the sediment-water interface. While riverine input may also contribute to surface Ni concentrations on the Chukchi Shelf, any correlation with f_{met} is overshadowed by the non-conservative biological cycling affecting Ni and other bioactive metals such as Zn, Cd, and Fe in the productive Chukchi Sea (Jensen, Morton, et al., 2020; Jensen et al., 2019; Zhang et al., 2019). Thus, benthic fluxes and potential preferential uptake by phytoplankton in the surface ocean appeared to drive the distribution of Ni over the Bering and Chukchi Shelves, in contrast to Cu.

The deeper CAA stations along GN02 and GN03 (~400 m) and the Barents Shelf (~200 m) along GN04 did not show benthic sources or appreciable increases of either Cu or Ni (Figures 2 and 3). Gerringa et al. (2021) found no evidence for sedimentary sources of Cu or Ni along the Barents Shelf during GN04, and any increase of Cu or Ni was surficial and could be attributed to low salinity and thus riverine sources. As has been previously postulated, the Barents Shelf is less productive and may be too deep to generate a significant benthic trace metal source (Jensen et al., 2019; Sakshaug, 2004). Sediment resuspension, rather than reductive dissolution, has been linked to Fe and Mn benthic fluxes along the CAA (Colombo et al., 2021), but this apparently did not meaningfully affect Cu and Ni, which shared no relationship to other dissolved trace metals in the CAA. The dominant feature in the CAA appeared to be the high dissolved Cu and Ni concentrations in the Canada Basin UHL waters that flow through the CAA and out into Baffin Bay.

4.2. Halocline (UHL)

Concentrations of Cu and Ni were elevated not only in the surface but also throughout the UHL observed along GN01 in the Canada Basin and into the CAA along GN03 and GN02 (Figures 2, 3, and 7), similar to previous findings (Cid et al., 2012; Jensen, Morton, et al., 2020; Jensen et al., 2019; Kondo et al., 2016). Within the UHL, Cu averaged 3.74 ± 0.26 nmol/kg, which was lower than its surface PML concentrations directly above (4.25 ± 0.29 nmol/kg; Figure 6a). In contrast, Ni averaged 7.08 ± 0.32 nmol/kg in the UHL of the Canada Basin, which was on average slightly higher than its surface average (6.73 ± 0.33 nmol/kg; Figure 6b). These UHL averages were within error of Chukchi Shelf bottom water concentrations (Figure 7), suggesting a connection between the shelf and concentrations offshore in the UHL. The UHL is formed from salty waters released during sea ice formation and brine rejection on the Chukchi Shelf (Shimada et al., 2005; Woodgate et al., 2005), which imparts high macronutrient and trace metal concentrations from shelf bottom waters that remain relatively undiluted during transit offshore (Jensen, Morton, et al., 2020; Jensen et al., 2019; Zhang et al., 2019).

The apparent increase in Ni but not Cu in the UHL compared to shelf bottom waters caused a deviation in the linear correlation between Cu and Ni at UHL depths (Figure 4b). Dissolved Cu and Ni were not significantly correlated in the UHL, with Ni positively correlated to the UHL tracer Si ($r^2 = 0.61$, $p < 0.01$, Figure S7e in

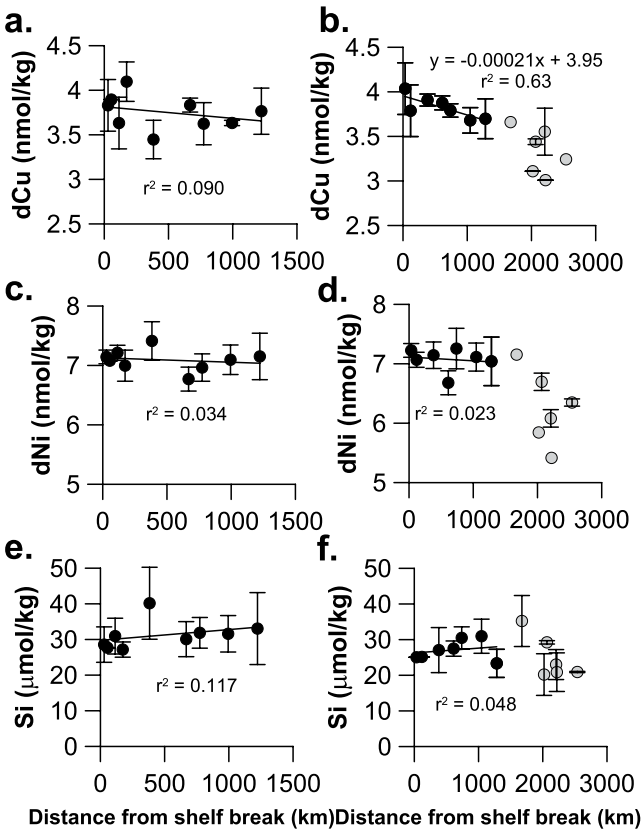

Figure 8. Plots of average Cu, Ni, and Si within the UHL (elevated Si, salinity 31–33.1) vs. distance from the 100 m isobath (shelf break) along GN01 (lefthand panels (a, c, e)) and GN01 into GN03/GN02 (righthand panels (b, d, f)). Stations used in (a, c, e) are GN01 Stations 8–19, 46–60 and in (b, d, f) GN01 Stations 65, 57, 60, GN03 Stations CAA8-CB4 (black dots) and GN02 Stations CAA3-CAA7 (gray dots). Correlations are shown for all relationships; only panel b had a statistically significant correlation between GN01 Station 60 to GN03 Station CAA8.

Supporting Information S1), while Cu was not correlated to Si (Figure S7b in Supporting Information S1). This Cu-Ni decoupling could occur either because Ni and Si are sourced together from the regeneration of phytoplankton detritus in Chukchi Shelf sediments without Cu (as suggested above) and/or that Cu is scavenged away in the UHL.

Thus, we tested the hypothesis that Cu is scavenged from the UHL layer during transport using a similar calculation as previous work that has shown rapid exponential scavenging of dissolved and particulate Fe and Mn near the shelf (Aguilar-Islas et al., 2013; Jensen, Morton, et al., 2020). Silicate is constant with distance from the shelf break, indicating that it is not net regenerated or scavenged. Thus, we compared averaged Cu or Ni within the bounds of the halocline (Si > 25 μmol/kg, salinity 31.0–33.1) at each of GN01 Stations 8–19, 46–60 to its distance from the 100 m isobath. Like Si, the results were approximately constant for each metal within error (Figures 8a and 8c), indicating that there was no substantial scavenging removal of Cu or Ni in the GN01 UHL within ~1,000 km of the Chukchi Shelf break. Thus, the observation above (Section 3.2.4) that the Chukchi Shelf provides a benthic source of Ni but not Cu is likely most responsible for the slight decoupling of Cu and Ni within the UHL.

We further probed the potential for scavenging by examining the persistence of both Cu and Ni within Pacific-origin water of the CAA. As has been observed previously, stations in the Canada Basin (CB2-CB4), the M'Clure Strait (CB1, Figure 1), and CAA have subsurface Si and trace metal maxima (Figure 3) commensurate with Canada Basin UHL water (Colombo et al., 2020; Jackson, 2017; Lehmann et al., 2019). Along GN02 and GN03, flow within the CAA was primarily eastward from M'Clure Strait to Baffin Bay, maintaining the UHL Si maximum between salinity 31.0 and 33.1. Dissolved Cu and Ni remained elevated in this water mass with average concentrations of 3.69 ± 0.20 nmol/kg and 6.89 ± 0.44 nmol/kg, respectively, between stations CB1-4 and CAA3-CAA8 where Si is >20 μmol/kg. However, UHL flow is known to recirculate within Barrow Strait, and therefore we truncated our UHL trends at GN03 Station CAA8, eastward of which Si was too low to distinguish the UHL. From the Chukchi Shelf 100 m isobath (Station 61) to CAA8 (1,675 km total distance), Cu decreased linearly ($r^2 = 0.63$, $p < 0.01$, Figure 8b) when plotted against distance, corresponding to a removal of 0.00021 nmol/kg Cu km^{-1}. Nickel had no relationship to distance but clearly decreased between stations CAA3-CAA7 (>2,000 km from the 100m isobath, Figure 8d, gray circles), as did Cu (Figure 8b). Silicate is shown as a comparison, demonstrating a relatively conservative pattern within the Canada Basin (Figure 8e) and a similar decrease between CAA3-CAA7 (Figure 8f, gray circles) due to conservative mixing. Thus, slow scavenging of Cu within the CAA (up until Station CAA8) may be responsible for the Cu decrease moving from the Canada Basin to Baffin Bay (Figure 4), while Ni and Si were only affected by mixing.

4.3. Atlantic Layer (AL)

Below the halocline, the AL (~250–600 m depth) originates in the Atlantic Ocean, flowing first through the Eastern Arctic and cycling slowly into the Western Arctic, traceable by a maximum in potential temperature (θ>0°C, Rudels, 2015). Tracking the inventory of Cu and Ni within this water mass as it ages allowed a distinction between conservative mixing of water masses (linear relationship with θ_{max} at each station), inputs of Cu and Ni (curved upward relationship with θ_{max}) such as by vertical biological regeneration inputs, or scavenging losses of Cu or Ni (curved downward relationship with θ_{max}). Previous studies found that nutrient-type metals such as Zn and Cd had a linear negative correlation with θ_{max} along GN01, indicating conservative mixing of low-Zn and -Cd Atlantic waters with the Zn- and Cd-rich halocline above (Jensen et al., 2019; Zhang et al., 2019). Given that Ni

Table 3
Average Deep Water Concentrations ± Standard Deviation

	Cu (nmol/kg)	Ni (nmol/kg)
Canada Basin (>1,800 m)	1.42 ± 0.11	3.09 ± 0.09
Makarov Basin (>1,800 m)	1.40 ± 0.11	3.15 ± 0.07
Amundsen Basin (>1,800 m)	1.56 ± 0.07	3.53 ± 0.08
Nansen Basin (>1,800 m)	1.59 ± 0.05	3.61 ± 0.10
All Arctic Basins (>1,800 m)	1.57 ± 0.47	3.40 ± 0.35
Global Average (>1,000 m)	2.60 ± 1.02	7.76 ± 1.56

Note. The composite Arctic average and standard deviation as well as the global average are shown for reference. Cruise transects GN01, GN03, and GN04 are included in this analysis where station depth exceeded 1,800 m.

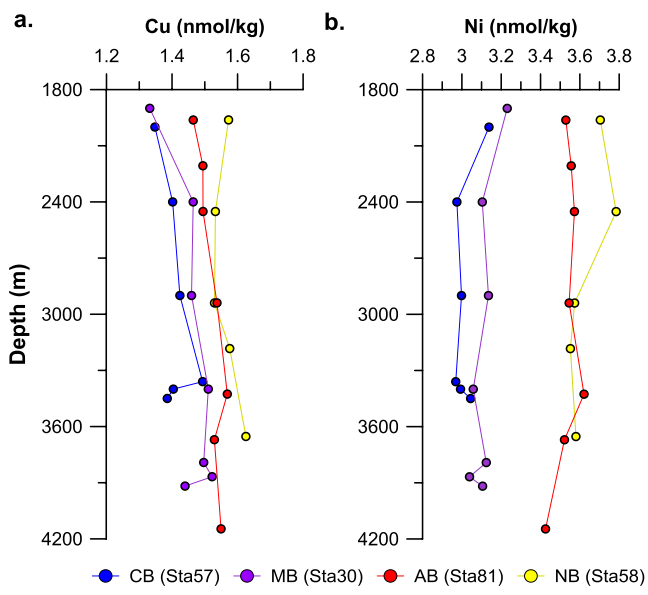

Figure 9. Copper and nickel in Arctic deep water. (a) Cu and (b) Ni below 1,800 m in the Canada Basin (CB, GN01 Station 57), Makarov Basin (MB, GN01 Station 30, purple), Amundsen Basin (AB, GN04 Station 81, red), and Nansen Basin (NB, GN04 Station 58, yellow). There is a clear disparity between the Eastern (NB and AB) and Western (CB and MB) Basins, particularly for Ni.

and Cu were elevated within the Western Arctic UHL, we expected a similar linear relationship to that observed for Zn and Cd.

Using data from GN01 and GN04 (Figure S8 in Supporting Information S1), we observed a flat linear relationship between Ni and θ_{max} (with two outliers), indicating no non-conservative additions to or losses from the AL and similar Ni concentrations in the UHL and AL. Notably, along GN04, where Atlantic water was a large component of water along the Barents Shelf and Nansen Basin (Gerringa et al., 2021), the θ_{max} was significantly higher (1°C –9°C) than at GN01 stations that were composed of older Atlantic waters already mixed with colder waters above or below.

However, the Cu trends in the AL were more complex. There was a negative linear relationship between Cu and θ_{max} along GN01 (Figure S8 in Supporting Information S1, blue dots), indicating conservative mixing between the high-Cu UHL waters and low-Cu Atlantic waters in the Western Arctic. However, the low-Cu AL trend was not borne out by the GN04 data set, which when combined with the GN01 AL data recorded no relationship between Cu and θ_{max} (Gerringa et al., 2021; Figure S8 in Supporting Information S1, blue and orange dots). Overall, these trends suggest that Cu and Ni are not appreciably scavenged or regenerated in the AL along the circulation pathway moving from the origin in the Barents Sea to the Chukchi Shelf. Importantly, a linearly decreasing relationship between AOU and θ_{max} was reported previously for the GN01 stations (Jensen et al., 2019), which underscores the minimal impact of vertical regeneration inputs for macronutrients or the micronutrients were study here; this is most likely explained by the oligotrophic conditions under the ice cover of the central Arctic (Black, 2018; Cai et al., 2010).

4.4. Deep Waters

Concentrations of Cu and Ni were low and homogenous in deep waters below 1,800 m, with Cu = 1.57 ± 0.47 nmol/kg and Ni = 3.40 ± 0.35 nmol/kg across the entire Arctic (Table 3). These were the lowest concentrations along all four Arctic GEOTRACES sections and represent a clear contrast to global averages for deep water Cu and Ni concentrations below 1,000 m, which are higher at 2.60 ± 1.02 and 7.76 ± 1.56 nmol/kg, respectively (Schlitzer et al., 2018). In Arctic deep waters, Cu and Ni concentrations encompass a range too small to allow a significant linear relationship between Cu and Ni below 1,800 m; however, these low concentrations do appear to "anchor" the overall GN01 Cu-Ni linear correlation in the Arctic (Figure 4).

Although deep water concentrations of Cu and Ni were low overall, they did vary slightly among the different Arctic Ocean basins: the Canada and Makarov basins (Western Arctic), and the Nansen and Amundsen basins (Eastern Arctic). The Lomonosov Ridge prohibits significant exchange between the Amundsen and Makarov basins below its 1,800 m sill, while the Alpha-Mendeleev Ridge between the Makarov and Canada and the Gakkel Ridge between the Nansen and Amundsen basins weakly restrict exchange below 2,200 and ~2,000 m, respectively (Jakobsson et al., 2012). Seawater is thought to circulate gradually from the deep Nansen Basin counterclockwise into the Amundsen, Makarov, and Canada Basins (Aagaard et al., 1985). Below 1,800 m, both Cu and Ni were higher in the younger Eastern basins compared to the older Western basins (Table 3, Figure 9, Gerringa et al., 2021).

The average Ni concentrations below 1,800 m were significantly different among the four basins (2-tailed t tests, $p < 0.05$) suggesting that Ni appreciably decreased in the deep water layers between the Nansen, Amundsen,

Makarov, and Canada basins. This indicates that Ni concentrations decreased as water circulates slowly between the basins on the timescale of centuries (Rudels et al., 2004; Tanhua et al., 2009; Timmermans et al., 2003). For Cu, only the decrease moving across the Lomonosov Ridge ($p < 0.05$) was statistically significant, and the spatial trends for both elements were driven primarily by noticeably higher concentrations of both Cu and Ni in the Nansen and Amundsen basins (Figure 9).

Arctic deep waters should be excellent indicators of metal scavenging, given their large age gradient (200–500 yr, Tanhua et al., 2009) and negligible vertical regeneration inputs given limited productivity under the sea ice cover, which often otherwise complicate deep water scavenging trends. Globally, Ni is thought to accumulate in deep waters with age following the remineralization of nutrients with depth and subsequent accumulation as deep waters age, creating distinct Ni deep water clusters at lower concentrations in the Atlantic and higher concentrations in the Pacific (Figure 4a). Arctic deep waters showed the opposite trend between Ni, Cu, and water mass age, namely that Ni and Cu both decreased with increasing age. Recent studies attribute this decrease in Ni and Cu concentration between the Eastern Arctic and Western Arctic to potential boundary scavenging and the presence of shelf ventilation in the Eastern Arctic (Gerringa et al., 2021). Indeed, the Chukchi Shelf and Western Arctic stations (GN01 and GN03) are more highly stratified, as evidenced by lower surface density and higher Brunt-Vaisala frequencies compared to the Barents Sea and Nansen Basin stations (GN04, Figure S9 in Supporting Information S1). This stratification in the Western Arctic likely provides a barrier to vertical convection in the shelf-slope region and thus to significant mixing of high nutrient/metal UHL waters into the Canada and Makarov basin deep waters.

Both Cu and Ni showed statistically significant differences between the younger, more ventilated Eastern Arctic basins (Nansen and Amundsen, 150–200 yr) and the older, more stratified Western Arctic basins (Makarov and Canada, 300–500 yr; Schlosser et al., 1994; Tanhua et al., 2009). Is this due to scavenging on the timescale of centuries? While this might be expected for Cu, Ni is not typically considering a scavenging-type element. We note that other elements (e.g., Cd [Zhang et al., 2019], Fe, Mn, Co, Zn [Bundy et al., 2020; Gerringa et al., 2021; Jensen, Morton, et al., 2020; Jensen et al., 2019]) also showed a decrease in deep water concentrations across basins, and since some of these elements are also not thought to be particle-reactive, we cannot definitively attribute this apparent loss of Cu or Ni to scavenging with age. Rather, differences in initial water mass composition during the mixing of waters that ultimately form Arctic deep water may help explain this trend, as has been proffered to explain Arctic deep water Si trends (Brzezinski et al., 2021) or shelf-slope ventilation as proposed in the Eastern Arctic (Gerringa et al., 2021).

Moreover, both Cu and Ni were affected by benthic nepheloid layers (BNLs) that were intermittently present along the GN01 transect. Although most full-depth stations (14, 19, 26, 30, 32, 38, 48, 52, 57) showed evidence of BNLs via a reduction in light transmission in the sensor data (Gardner et al., 2018), particulate aluminum in the large size fraction, a chemical metric of BNL lithogenic sediment resuspension, was particularly elevated at Stations 14, 19, 26, 30, 32, 48, and 57 (Xiang & Lam, 2020). At these stations, Cu and Ni both showed variations in the bottom-most samples. At Stations 30, 32, 48, and 57, dissolved Cu decreased, and Ni increased sharply in the BNL (Figure S10 in Supporting Information S1), showcasing the common dynamic of benthic nepheloid layers (BNLs): scavenging of dissolved Cu (Jacquot & Moffett, 2015; Sherrell & Boyle, 1992) and resuspension-driven additions of nutrient-type elements like Ni (Löscher, 1999; Sherrell & Boyle, 1992). In contrast, at stations 14, 19, and 26, dissolved Cu was slightly elevated near the bottom, indicating potential release from resuspended sediments (Boyle et al., 1977), while Ni appeared to decrease toward the seafloor. This could be a result of Ni scavenging onto central Arctic Mn-rich sediments (März et al., 2011), as positively charged Ni in seawater (Byrne, 2002) is expected to adsorb onto the slightly negatively charged surfaces of Mn oxides moreso than organically bound Cu, which prefers Fe oxide surfaces (Koschinsky & Hein, 2003). A further analysis of spatial differences in either removal or addition of dissolved Cu and Ni in the BNLs along GN01 requires a more detailed spatial survey of Arctic sediment geochemistry, particularly the distribution of Mn vs. Fe oxides in sediments that might locally and differentially scavenge these metals.

5. Conclusions

Dissolved Cu and Ni display a globally unprecedented linear relationship across the Arctic Ocean that reflects the unique fluxes into this basin and the unique distributions of trace metals. The profile shapes for Ni and Cu are noticeably different in the Arctic than in other ocean basins, with high surface concentrations far surpassing

global averages and a decrease with depth to low and homogenous concentrations below 1,000 m. This aligns well with studies of other metals in the Western Arctic, in particular Mn and Co, both of which have a similar profile shape to Cu and Ni (Bundy et al., 2020; Jensen, Morton, et al., 2020), as well as metals in the Eastern Arctic (Gerringa et al., 2021), pointing to Arctic-specific fluxes and water mass advection and mixing that form these unique metal distributions.

We conclude that the linear correlation between Cu and Ni across the pan-Arctic is driven predominantly by significant riverine fluxes for both Cu and Ni, particularly within the TPD. Rivers must be considered in any oceanic model of Cu or Ni biogeochemistry. In addition, we discovered that benthic porewater fluxes associated with the sediment regeneration of organic matter are also an important source for Ni into bottom waters of the Bering and Chukchi Shelves along GN01, which are eventually entrained into the UHL of the open Western Arctic. In contrast, Cu showed no benthic margin source or evidence of surface biological uptake and instead remained correlated to river input. This is opposite to the pattern expected from previous investigations, where benthic sources have long been considered for Cu but were underemphasized for Ni. However, riverine and benthic sources are particularly prevalent in the Western Arctic Ocean, with significant freshwater volume accumulation in surface waters (Carmack et al., 2008; Yamamoto-Kawai et al., 2008) and on the shallow Chukchi Shelf (Jakobsson et al., 2004). The TPD bisecting the Arctic is also a notable feature for trace metals in the surface Makarov and Amundsen basins (Charette et al., 2020). In particular, our conclusion that the riverine fluxes are the dominant control on Cu in the PML in this region aligns well with current literature suggesting that the river flux of Cu is far greater and more dominant than previously established, decreasing the residence time of Cu in the ocean considerably (Richon & Tagliabue, 2019).

Removal by scavenging in surface and intermediate waters such as the UHL or AL appears possible for Cu only within the CAA and was not observed for Ni. Previous work shows removal of non-scavenged-type elements in the Arctic deep waters, in line with the observation of this study that dissolved Cu and Ni concentrations decreased across the four Arctic basins with increasing age over century timescales. While this may be due to shelf-slope ventilation or changes in initial water mass concentrations that mixed in these basins during deep water formation, scavenging of both Cu and Ni cannot be precluded by our deep water observations, and it is notable that Ni scavenging has been hypothesized to occur onto Mn oxides (Koschinsky & Hein, 2003) and in the Mediterranean Sea (Middag et al., 2022).

More work is needed on Arctic Cu and Ni distributions, as well as the chemical complexation of Cu and Ni, to demonstrate whether this coupled Cu-Ni behavior is merely a reflection of processes endemic to the Arctic Ocean where freshwater sources are dominant and vertical biological pump processes are weak. Indeed, there were no discernible effects from biological uptake and remineralization across the Arctic basins and within the CAA off-shelf. Given the impact of river outflow on Cu and Ni concentrations, we may expect increased Arctic freshening to bring higher levels of Cu and Ni into the surface Arctic in future. Further studies evaluating freshwater anomalies in the North Atlantic resulting from a freshening Arctic Ocean should note the geochemical impact of high Cu and Ni present in Arctic rivers and productive shelves.

Data Availability Statement

All dissolved metal, nutrient, and stable isotope data from GN01, GN02, GN03, and GN04 described above are available in a consolidated form as part of the GEOTRACES Intermediate Data Product 2021, available for free download at https://www.geotraces.org/geotraces-intermediate-data-product-2021/. Note that the sole exception is the macronutrient data for GN04 available at https://doi.org/10.1594/PANGAEA.868396. Individual data sets may be found at: GN01 metals (https://doi.org/10.26008/1912/bco-dmo.817259.2), GN01 hydrography and nutrients (https://doi.org/10.1575/1912/bco-dmo.647259.4 and https://doi.org/10.1594/IEDA/100633), GN04 (https://doi.org/10.25850/nioz/7b.b.jc), GN02/03 (https://dspace.library.uvic.ca/handle/1828/8920).

Acknowledgments
The authors would like to thank and acknowledge the Captain and crew of the USCGC *Healy*, Chief Scientists Dave Kadko, William Landing, and Greg Cutter for proposing and enabling cruise leadership, Chief Scientist Ursula Schauer and Captain Schwarze, and the crew of FS *Polarstern* on GN04, and Chief Scientist Roger François and the captain and crew of the *CCGS Amundsen*. This work would not have been possible without the GN01 Supertechnicians Gabi Weiss and Simone Moos and GN02/GN03 trace metal group (Priyanka Chandan, Kang Wang, Kathleen Munson, Jingxuan Li, David Semeniuk, Dave Janssen, Rowan Fox, and Kathryn Purdon) for sample collection at sea. The authors thank Luz Romero for assistance with ICP-MS analyses and maintenance and Angelica Pasqualini, Bob Newton, Peter Schlosser, Tobias Koffman, Helmuth Thomas, and Alfonso Mucci for contribution of their oxygen isotope measurements and freshwater model estimates used to quantify fractional sea ice melt and meteoric water. Additionally, this work would not have been possible without the SIO ODF team for nutrient and salinity analyses during GN01. This work was supported by NSF Division of Ocean Sciences (OCE) awards 1434493 and 1713677 to JNF and RMS and the NWO under contract number 822.01.018 to L.J.A. Gerringa. D. Bauch was funded for this project by DFG (BA1689/2-2). The International GEOTRACES Programme is possible in part thanks to the support from the U.S. National Science Foundation (OCE1840868) to the Scientific Committee on Oceanic Research (SCOR).

References

Aagaard, K., Coachman, L., & Carmack, E. (1981). On the halocline of the Arctic Ocean. *Deep Sea Research Part A. Oceanographic Research Papers*, *28*(6), 529–545. https://doi.org/10.1016/0198-0149(81)90115-1

Aagaard, K., Swift, J. H., & Carmack, E. C. (1985). Thermohaline circulation in the Arctic Mediterranean Seas. *Journal of Geophysical Research: Oceans*, *90*(C3), 4833–4846. https://doi.org/10.1029/jc090ic03p04833

Abualhaija, M. M., Whitby, H., & van den Berg, C. M. G. (2015). Competition between copper and iron for humic ligands in estuarine waters. *Marine Chemistry*, *172*, 46–56. https://doi.org/10.1016/j.marchem.2015.03.010

Aguilar-Islas, A. M., Rember, R., Nishino, S., Kikuchi, T., & Itoh, M. (2013). Partitioning and lateral transport of iron to the Canada Basin. *Polar Science*, *7*(2), 82–99. https://doi.org/10.1016/j.polar.2012.11.001

Aguilar-Islas, A. M., Rember, R. D., Mordy, C. W., & Wu, J. (2008). Sea ice-derived dissolved iron and its potential influence on the spring algal bloom in the Bering Sea. *Geophysical Research Letters*, *35*(24). https://doi.org/10.1029/2008gl035736

Anderson, L. G., Andersson, P. S., Björk, G., Peter Jones, E., Jutterström, S., & Wåhlström, I. (2013). Source and formation of the upper halocline of the Arctic Ocean. *Journal of Geophysical Research: Oceans*, *118*(1), 410–421. https://doi.org/10.1029/2012jc008291

Annett, A. L., Lapi, S., Ruth, T. J., & Maldonado, M. T. (2008). The effects of Cu and Fe availability on the growth and Cu: C ratios of marine diatoms. *Limnology and Oceanography*, *53*(6), 2451–2461. https://doi.org/10.4319/lo.2008.53.6.2451

Bacon, M. P., & Anderson, R. F. (1982). Distribution of thorium isotopes between dissolved and particulate forms in the deep sea. *Journal of Geophysical Research: Oceans*, *87*(C3), 2045–2056. https://doi.org/10.1029/jc087ic03p02045

Bauch, D., van der Loeff, M. R., Andersen, N., Torres-Valdes, S., Bakker, K., & Abrahamsen, E. P. (2011). Origin of freshwater and polynya water in the Arctic Ocean halocline in summer 2007. *Progress in Oceanography*, *91*(4), 482–495. https://doi.org/10.1016/j.pocean.2011.07.017

Biller, D. V., & Bruland, K. W. (2013). Sources and distributions of Mn, Fe, Co, Ni, Cu, Zn, and Cd relative to macronutrients along the central California coast during the spring and summer upwelling season. *Marine Chemistry*, *155*, 50–70. https://doi.org/10.1016/j.marchem.2013.06.003

Black, E. E. (2018). *An investigation of basin-scale controls on upper ocean export and remineralization*. Massachusetts Institute of Technology.

Boiteau, R. M., Till, C. P., Ruacho, A., Bundy, R. M., Hawco, N. J., McKenna, A. M., et al. (2016). Structural characterization of natural nickel and copper binding ligands along the US GEOTRACES eastern Pacific zonal transect. *Frontiers in Marine Science*, *3*(243). https://doi.org/10.3389/fmars.2016.00243

Böning, P., Shaw, T., Pahnke, K., & Brumsack, H.-J. (2015). Nickel as indicator of fresh organic matter in upwelling sediments. *Geochimica et Cosmochimica Acta*, *162*, 99–108.

Bowie, A. R., Whitworth, D. J., Achterberg, E. P., Mantoura, R. F. C., & Worsfold, P. J. (2002). Biogeochemistry of Fe and other trace elements (Al, Co, Ni) in the upper Atlantic Ocean. *Deep Sea Research Part I: Oceanographic Research Papers*, *49*(4), 605–636. https://doi.org/10.1016/s0967-0637(01)00061-9

Boyle, E. A., Huested, S. S., & Jones, S. P. (1981). On the distribution of copper, nickel, and cadmium in the surface waters of the North Atlantic and North Pacific Ocean. *Journal of Geophysical Research: Oceans*, *86*(C9), 8048–8066. https://doi.org/10.1029/jc086ic09p08048

Boyle, E. A., Sclater, F., & Edmond, J. (1977). The distribution of dissolved copper in the Pacific. *Earth and Planetary Science Letters*, *37*(1), 38–54. https://doi.org/10.1016/0012-821x(77)90144-3

Broering, E. P., Truong, P. T., Gale, E. M., & Harrop, T. C. (2013). Synthetic analogs of nickel superoxide dismutase: A new role for nickel in biology. *Biochemistry*, *52*(1), 4–18. https://doi.org/10.1021/bi3014533

Bruland, K. W. (1980). Oceanographic distributions of cadmium, zinc, nickel, and copper in the North Pacific. *Earth and Planetary Science Letters*, *47*(2), 176–198. https://doi.org/10.1016/0012-821x(80)90035-7

Bruland, K. W., Middag, R., & Lohan, M. C. (2014). 8.2-controls of trace metals in seawater. In H. D. Holland, & K. K. Turekian (Eds.), *Treatise on geochemistry* (2nd ed., pp. 19–51). Elsevier. https://doi.org/10.1016/b978-0-08-095975-7.00602-1

Brzezinski, M. A., Closset, I., Jones, J. L., de Souza, G. F., & Maden, C. (2021). New constraints on the physical and biological controls on the silicon isotopic composition of the Arctic Ocean. *Frontiers in Marine Science*, *8*. https://doi.org/10.3389/fmars.2021.699762

Bundy, R. M., Tagliabue, A., Hawco, N. J., Morton, P. L., Twining, B. S., Hatta, M., et al. (2020). Elevated sources of cobalt in the Arctic Ocean. *Biogeosciences Discuss*, *17*, 4745–4767. https://doi.org/10.5194/bg-17-4745-2020

Byrne, R. H. (2002). Inorganic speciation of dissolved elements in seawater: The influence of pH on concentration ratios. *Geochemical Transactions*, *3*(1), 11. https://doi.org/10.1186/1467-4866-3-11

Cai, P., Rutgers Van Der Loeff, M., Stimac, I., Nöthig, E. M., Lepore, K., & Moran, S. (2010). Low export flux of particulate organic carbon in the central Arctic Ocean as revealed by ^{234}Th: ^{238}U disequilibrium. *Journal of Geophysical Research: Oceans*, *115*(C10). https://doi.org/10.1029/2009jc005595

Cameron, V., & Vance, D. (2014). Heavy nickel isotope compositions in rivers and the oceans. *Geochimica et Cosmochimica Acta*, *128*, 195–211. https://doi.org/10.1016/j.gca.2013.12.007

Carmack, E., McLaughlin, F., Yamamoto-Kawai, M., Itoh, M., Shimada, K., Krishfield, R., & Proshutinsky, A. (2008). Freshwater storage in the northern ocean and the special role of the Beaufort Gyre. In *Arctic-subArctic ocean fluxes* (pp. 145–169). Springer. https://doi.org/10.1007/978-1-4020-6774-7_8

Charette, M. A., Kipp, L. E., Jensen, L. T., Dabrowski, J. S., Whitmore, L. M., Fitzsimmons, J. N., et al. (2020). The Transpolar Drift as a source of riverine and shelf-derived trace elements to the central Arctic Ocean. *Journal of Geophysical Research: Oceans*, *125*, e2019JC015920

Cid, A. P., Nakatsuka, S., & Sohrin, Y. (2012). Stoichiometry among bioactive trace metals in the Chukchi and Beaufort Seas. *Journal of Oceanography*, *68*(6), 985–1001. https://doi.org/10.1007/s10872-012-0150-8

Coachman, L. K., & Barnes, C. A. (1963). The movement of Atlantic water in the Arctic Ocean. *Arctic*, *16*(1), 1–80. https://doi.org/10.14430/arctic3517

Coale, K. H., & Bruland, K. W. (1988). Copper complexation in the northeast Pacific. *Limnology and Oceanography*, *33*(5), 1084–1101. https://doi.org/10.4319/lo.1988.33.5.1084

Colombo, M., Jackson, S. L., Cullen, J. T., & Orians, K. J. (2020). Dissolved iron and manganese in the Canadian Arctic Ocean: On the biogeochemical processes controlling their distributions. *Geochimica et Cosmochimica Acta*, *277*, 150–174. https://doi.org/10.1016/j.gca.2020.03.012

Colombo, M., Rogalla, B., Li, J., Allen, S. E., Orians, K. J., & Maldonado, M. T. (2021). Canadian Arctic Archipelago shelf-ocean interactions: A major iron source to Pacific derived waters transiting to the Atlantic. *Global Biogeochemical Cycles*, *35*(10), e2021GB007058. https://doi.org/10.1029/2021gb007058

Cutter, G. A., Andersson, P., Codispoti, L., Croot, P., Francois, R., Lohan, M., et al. (2010). *Sampling and sample-handling protocols for GEOTRACES cruises*. GEOTRACES.

Cutter, G. A., & Bruland, K. W. (2012). Rapid and noncontaminating sampling system for trace elements in global ocean surveys. *Limnology and Oceanography: Methods*, *10*(6), 425–436. https://doi.org/10.4319/lom.2012.10.425

Danielsson, L.-G., Magnusson, B., & Westerlund, S. (1985). Cadmium, copper, iron, nickel, and zinc in the north-east Atlantic Ocean. *Marine Chemistry*, *17*(1), 23–41. https://doi.org/10.1016/0304-4203(85)90034-9

Dickson, R. J., & Hunter, K. A. (1981). Copper and nickel in surface waters of Otago Harbour. *New Zealand Journal of Marine and Freshwater Research*, *15*(4), 475–480. https://doi.org/10.1080/00288330.1981.9515939

Donat, J. R., Lao, K. A., & Bruland, K. W. (1994). Speciation of dissolved copper and nickel in South San Francisco Bay: A multi-method approach. *Analytica Chimica Acta*, *284*(3), 547–571. https://doi.org/10.1016/0003-2670(94)85061-5

Dupont, C. L., Barbeau, K., & Palenik, B. (2008). Ni uptake and limitation in marine synechococcus strains. *Applied and Environmental Microbiology*, *74*(1), 23–31. https://doi.org/10.1128/aem.01007-07

Eicken, H., Krouse, H., Kadko, D., & Perovich, D. (2002). Tracer studies of pathways and rates of meltwater transport through Arctic summer sea ice. *Journal of Geophysical Research: Oceans*, *107*(C10). https://doi.org/10.1029/2000jc000583

Ekwurzel, B., Schlosser, P., Mortlock, R. A., Fairbanks, R. G., & Swift, J. H. (2001). River runoff, sea ice meltwater, and Pacific water distribution and mean residence times in the Arctic Ocean. *Journal of Geophysical Research: Oceans*, *106*(C5), 9075–9092. https://doi.org/10.1029/1999jc000024

Epstein, S., & Mayeda, T. (1953). Variation of O^{18} content of waters from natural sources. *Geochimica et Cosmochimica Acta*, *4*(5), 213–224. https://doi.org/10.1016/0016-7037(53)90051-9

Gardner, W. D., Richardson, M. J., & Mishonov, A. V. (2018). Global assessment of benthic nepheloid layers and linkage with upper ocean dynamics. *Earth and Planetary Science Letters*, *482*(Supplement C), 126–134. https://doi.org/10.1016/j.epsl.2017.11.008

Gerringa, L. J. A., Rijkenberg, M. J. A., Slagter, H. A., Laan, P., Paffrath, R., Bauch, D., et al. (2021). Dissolved Cd, Co, Cu, Fe, Mn, Ni, and Zn in the Arctic Ocean. *Journal of Geophysical Research: Oceans*, e2021JC017323. https://doi.org/10.1029/2021jc017323

Gerringa, L. J. A., van der Meer, J., & Cauwet, G. (1991). Complexation of copper and nickel in the dissolved phase of marine sediment slurries. *Marine Chemistry*, *36*(1), 51–70. https://doi.org/10.1016/s0304-4203(09)90054-8

Granger, J., & Ward, B. B. (2003). Accumulation of nitrogen oxides in copper-limited cultures of denitrifying bacteria. *Limnology and Oceanography*, *48*(1), 313–318. https://doi.org/10.4319/lo.2003.48.1.0313

Grasshoff, K., Kremling, K., & Ehrhardt, M. (2009). *Methods of seawater analysis*. John Wiley & Sons.

Guay, C. K., McLaughlin, F. A., & Yamamoto-Kawai, M. (2009). Differentiating fluvial components of upper Canada Basin waters on the basis of measurements of dissolved barium combined with other physical and chemical tracers. *Journal of Geophysical Research: Oceans*, *114*(C1). https://doi.org/10.1029/2008jc005099

Heggie, D. T. (1982). Copper in surface waters of the Bering Sea. *Geochimica et Cosmochimica Acta*, *46*(7), 1301–1306. https://doi.org/10.1016/0016-7037(82)90014-x

Heggie, D. T., Klinkhammer, G., & Cullen, D. (1987). Manganese and copper fluxes from continental margin sediments. *Geochimica et Cosmochimica Acta*, *51*(5), 1059–1070. https://doi.org/10.1016/0016-7037(87)90200-6

Hines, M. E., Berry Lyons, W., Armstrong, P. B., Orem, W. H., Spencer, M. J., Gaudette, H. E., & Jones, G. E. (1984). Seasonal metal remobilization in the sediments of Great Bay, New Hampshire. *Marine Chemistry*, *15*(2), 173–187. https://doi.org/10.1016/0304-4203(84)90014-8

Ho, T.-Y. (2013). Nickel limitation of nitrogen fixation in Trichodesmium. *Limnology and Oceanography*, *58*(1), 112–120. https://doi.org/10.4319/lo.2013.58.1.0112

Hölemann, J., Schirmacher, M., & Prange, A. (1999). Dissolved and particulate major and trace elements in newly formed ice from the Laptev Sea (Transdrift III, October 1995). In *Land-ocean systems in the Siberian Arctic* (pp. 101–111). Springer.

Hydes, D., Aoyama, M., Aminot, A., Bakker, K., Becker, S., Coverly, S., et al. (2010). Determination of dissolved nutrients (N, P, Si) in seawater with high precision and inter-comparability using gas-segmented continuous flow analyzers.

Irving, H., & Williams, R. J. P. (1953). The stability of transition-metal complexes. *Journal of the Chemical Society*, *637*, 3192–3210. https://doi.org/10.1039/jr9530003192

Jackson, S. (2017). *The distribution of dissolved cadmium in the Canadian Arctic Ocean (Dissertation thesis)*. University of Victoria. Retrieved from http://hdl.handle.net/1828/8920

Jackson, S. L., Spence, J., Janssen, D. J., Ross, A. R. S., & Cullen, J. T. (2018). Determination of Mn, Fe, Ni, Cu, Zn, Cd, and Pb in seawater using offline extraction and triple quadrupole ICP-MS/MS. *Journal of Analytical Atomic Spectrometry*, *33*(2), 304–313. https://doi.org/10.1039/c7ja00237h

Jacquot, J. E., & Moffett, J. W. (2015). Copper distribution and speciation across the International GEOTRACES section GA03. *Deep Sea Research Part II: Topical Studies in Oceanography*, *116*, 187–207. https://doi.org/10.1016/j.dsr2.2014.11.013

Jakobsson, M., Grantz, A., Kristoffersen, Y., Macnab, R., MacDonald, R., Sakshaug, E., et al. (2004). The Arctic Ocean: Boundary conditions and background information. In *The organic carbon cycle in the Arctic Ocean*, (pp. 1–32). Springer. https://doi.org/10.1007/978-3-642-18912-8_1

Jakobsson, M., Mayer, L., Coakley, B., Dowdeswell, J. A., Forbes, S., Fridman, B., et al. (2012). The International Bathymetric Chart of the Arctic Ocean (IBCAO) version 3.0. *Geophysical Research Letters*, *39*(12), L12609. https://doi.org/10.1029/2012gl052219

Jensen, L. T., Morton, P., Twining, B. S., Heller, M. I., Hatta, M., Measures, C. I., et al. (2020). A comparison of marine Fe and Mn cycling: US GEOTRACES GN01 Western Arctic case study. *Geochimica et Cosmochimica Acta*, *288*, 138–160. https://doi.org/10.1016/j.gca.2020.08.006

Jensen, L. T., Wyatt, N. J., Landing, W. M., & Fitzsimmons, J. N. (2020). Assessment of the stability, sorption, and exchangeability of marine dissolved and colloidal metals. *Marine Chemistry*, *220*, 103754. https://doi.org/10.1016/j.marchem.2020.103754

Jensen, L. T., Wyatt, N. J., Twining, B. S., Rauschenberg, S., Landing, W. M., Sherrell, R. M., & Fitzsimmons, J. N. (2019). Biogeochemical cycling of dissolved zinc in the Western Arctic (Arctic GEOTRACES GN01). *Global Biogeochemical Cycles*, *33*(3), 343–369. https://doi.org/10.1029/2018gb005975

Jones, E. P., & Anderson, L. G. (1986). On the origin of the chemical properties of the Arctic Ocean halocline. *Journal of Geophysical Research: Oceans*, *91*(C9), 10759–10767. https://doi.org/10.1029/jc091ic09p10759

Kadko, D., Galfond, B., Landing, W. M., & Shelley, R. U. (2016). Determining the pathways, fate, and flux of atmospherically derived trace elements in the Arctic ocean/ice system. *Marine Chemistry*, *182*(Supplement C), 38–50. https://doi.org/10.1016/j.marchem.2016.04.006

Klunder, M. B., Bauch, D., Laan, P., de Baar, H. J. W., van Heuven, S., & Ober, S. (2012). Dissolved iron in the Arctic shelf seas and surface waters of the central Arctic Ocean: Impact of Arctic river water and ice-melt. *Journal of Geophysical Research: Oceans*, *117*(C1). https://doi.org/10.1029/2011jc007133

Klunder, M. B., Laan, P., Middag, R., de Baar, H. J. W., & Bakker, K. (2012). Dissolved iron in the Arctic Ocean: Important role of hydrothermal sources, shelf input, and scavenging removal. *Journal of Geophysical Research: Oceans*, *117*(C4). https://doi.org/10.1029/2011jc007135

Kondo, Y., Obata, H., Hioki, N., Ooki, A., Nishino, S., Kikuchi, T., & Kuma, K. (2016). Transport of trace metals (Mn, Fe, Ni, Zn, and Cd) in the Western Arctic Ocean (Chukchi Sea and Canada Basin) in late summer 2012. *Deep Sea Research Part I: Oceanographic Research Papers*, *116*, 236–252. https://doi.org/10.1016/j.dsr.2016.08.010

Koschinsky, A., & Hein, J. R. (2003). Uptake of elements from seawater by ferromanganese crusts: Solid-phase associations and seawater speciation. *Marine Geology*, *198*(3), 331–351. https://doi.org/10.1016/s0025-3227(03)00122-1

Krumpen, T., Belter, H. J., Boetius, A., Damm, E., Haas, C., Hendricks, S., et al. (2019). Arctic warming interrupts the Transpolar Drift and affects long-range transport of sea ice and ice-rafted matter. *Scientific Reports*, *9*(1), 1–9. https://doi.org/10.1038/s41598-019-41456-y

Lagerström, M. E., Field, M. P., Séguret, M., Fischer, L., Hann, S., & Sherrell, R. M. (2013). Automated on-line flow-injection ICP-MS determination of trace metals (Mn, Fe, Co, Ni, Cu, and Zn) in open ocean seawater: Application to the GEOTRACES program. *Marine Chemistry*, *155*, 71–80.

Laglera, L. M., Sukekava, C., Slagter, H. A., Downes, J., Aparicio-Gonzalez, A., & Gerringa, L. J. A. (2019). First quantification of the controlling role of humic substances in the transport of iron across the surface of the Arctic Ocean. *Environmental Science & Technology*, *53*(22), 13136–13145. https://doi.org/10.1021/acs.est.9b04240

Laglera, L. M., & van den Berg, C. M. (2003). Copper complexation by thiol compounds in estuarine waters. *Marine Chemistry*, *82*(1–2), 71–89. https://doi.org/10.1016/s0304-4203(03)00053-7

Lannuzel, D., Vancoppenolle, M., Van der Merwe, P., De Jong, J., Meiners, K. M., Grotti, M., et al. (2016). Iron in sea ice: Review and new insights. *Elementa: Science of the Anthropocene*, *4*, 000130. https://doi.org/10.12952/journal.elementa.000130

Lehmann, N., Kienast, M., Granger, J., Bourbonnais, A., Altabet, M., & Tremblay, J. É. (2019). Remote Western Arctic nutrients fuel remineralization in deep Baffin Bay. *Global Biogeochemical Cycles*, *33*(6), 649–667. https://doi.org/10.1029/2018gb006134

Little, S. H., Archer, C., McManus, J., Najorka, J., Wegorzewski, A. V., & Vance, D. (2020). Towards balancing the oceanic Ni budget. *Earth and Planetary Science Letters*, *547*, 116461. https://doi.org/10.1016/j.epsl.2020.116461

Löscher, B. M. (1999). Relationships among Ni, Cu, Zn, and major nutrients in the Southern Ocean. *Marine Chemistry*, *67*(1), 67–102.

Maldonado, M. T., Allen, A. E., Chong, J. S., Lin, K., Leus, D., Karpenko, N., & Harris, S. L. (2006). Copper-dependent iron transport in coastal and oceanic diatoms. *Limnology and Oceanography*, *51*(4), 1729–1743. https://doi.org/10.4319/lo.2006.51.4.1729

Marsay, C. M., Aguilar-Islas, A., Fitzsimmons, J. N., Hatta, M., Jensen, L. T., John, S. G., et al. (2018). Dissolved and particulate trace elements in late summer Arctic melt ponds. *Marine Chemistry*, *204*, 70–85. https://doi.org/10.1016/j.marchem.2018.06.002

März, C., Stratmann, A., Matthiessen, J., Meinhardt, A. K., Eckert, S., Schnetger, B., et al. (2011). Manganese-rich brown layers in Arctic Ocean sediments: Composition, formation mechanisms, and diagenetic overprint. *Geochimica et Cosmochimica Acta*, *75*(23), 7668–7687.

Measures, C. (1999). The role of entrained sediments in sea ice in the distribution of aluminum and iron in the surface waters of the Arctic Ocean. *Marine Chemistry*, *68*(1–2), 59–70. https://doi.org/10.1016/s0304-4203(99)00065-1

Middag, R., de Baar, H. J., Bruland, K. W., & van Heuven, S. M. (2020). The distribution of nickel in the west-Atlantic Ocean, its relationship with phosphate and a comparison to cadmium and zinc. *Frontiers in Marine Science*, *7*, 105. https://doi.org/10.3389/fmars.2020.00105

Middag, R., de Baar, H. J. W., Laan, P., & Klunder, M. B. (2011). Fluvial and hydrothermal input of manganese into the Arctic Ocean. *Geochimica et Cosmochimica Acta*, *75*(9), 2393–2408. https://doi.org/10.1016/j.gca.2011.02.011

Middag, R., Rolison, J. M., George, E., Gerringa, L. J. A., Rijkenberg, M. J. A., & Stirling, C. H. (2022). Basin-scale distributions of dissolved manganese, nickel, zinc, and cadmium in the Mediterranean Sea. *Marine Chemistry*, *238*, 104063. https://doi.org/10.1016/j.marchem.2021.104063

Miller, L. A., Papakyriakou, T. N., Collins, R. E., Deming, J. W., Ehn, J. K., Macdonald, R. W., et al. (2011). Carbon dynamics in sea ice: A winter flux time series. *Journal of Geophysical Research: Oceans*, *116*(C2). https://doi.org/10.1029/2009jc006058

Moffett, J. W., & Brand, L. E. (1996). Production of strong, extracellular Cu chelators by marine cyanobacteria in response to Cu stress. *Limnology and Oceanography*, *41*(3), 388–395. https://doi.org/10.4319/lo.1996.41.3.0388

Moffett, J. W., Brand, L. E., Croot, P. L., & Barbeau, K. A. (1997). Cu speciation and cyanobacterial distribution in harbors subject to anthropogenic Cu inputs. *Limnology and Oceanography*, *42*(5), 789–799. https://doi.org/10.4319/lo.1997.42.5.0789

Moore, R. M. (1978). The distribution of dissolved copper in the eastern Atlantic Ocean. *Earth and Planetary Science Letters*, *41*(4), 461–468. https://doi.org/10.1016/0012-821x(78)90177-2

Moore, R. M. (1981). Oceanographic distributions of zinc, cadmium, copper, and aluminium in waters of the central arctic. *Geochimica et Cosmochimica Acta*, *45*(12), 2475–2482. https://doi.org/10.1016/0016-7037(81)90099-5

Newton, R., Schlosser, P., Mortlock, R., Swift, J., & MacDonald, R. (2013). Canadian basin freshwater sources and changes: Results from the 2005 Arctic Ocean section. *Journal of Geophysical Research: Oceans*, *118*(4), 2133–2154. https://doi.org/10.1002/jgrc.20101

Nolting, R. F., & de Baar, H. J. W. (1994). Behavior of nickel, copper, zinc, and cadmium in the upper 300 m of a transect in the Southern Ocean (57°–62°S, 49°W). *Marine Chemistry*, *45*(3), 225–242. https://doi.org/10.1016/0304-4203(94)90006-x

Noriki, S., Arashitani, Y., Minakawa, M., Harada, K., & Tsunogai, S. (1998). Vertical cycling of Cu and Ni in the western North and equatorial Pacific. *Marine Chemistry*, *59*(3–4), 211–218. https://doi.org/10.1016/s0304-4203(97)00098-4

Opsahl, S., Benner, R., & Amon, R. M. W. (1999). Major flux of terrigenous dissolved organic matter through the Arctic Ocean. *Limnology and Oceanography*, *44*(8), 2017–2023. https://doi.org/10.4319/lo.1999.44.8.2017

Paffrath, R., Laukert, G., Bauch, D., van der Loeff, M. R., & Pahnke, K. (2021). Separating individual contributions of major Siberian rivers in the Transpolar Drift of the Arctic Ocean. *Scientific Reports*, *11*(1), 1–11. https://doi.org/10.1038/s41598-021-86948-y

Price, N., & Morel, F. M. (1991). Colimitation of phytoplankton growth by nickel and nitrogen. *Limnology and Oceanography*, *36*(6), 1071–1077. https://doi.org/10.4319/lo.1991.36.6.1071

Proshutinsky, A., Krishfield, R., Timmermans, M. L., Toole, J., Carmack, E., McLaughlin, F., et al. (2009). Beaufort Gyre freshwater reservoir: State and variability from observations. *Journal of Geophysical Research: Oceans*, *114*(C1). https://doi.org/10.1029/2008jc005104

Richon, C., & Tagliabue, A. (2019). Insights into the major processes driving the global distribution of copper in the ocean from a global model. *Global Biogeochemical Cycles*, *33*(12), 1594–1610. https://doi.org/10.1029/2019gb006280

Rijkenberg, M. J. A., Slagter, H. A., van der Rutgers Loeff, M., van Ooijen, J., & Gerringa, L. J. A. (2018). Dissolved Fe in the deep and upper Arctic Ocean with a focus on Fe limitation in the Nansen Basin. *Frontiers in Marine Science*, *5*(88). https://doi.org/10.3389/fmars.2018.00088

Rudels, B. (2015). Arctic Ocean circulation, processes, and water masses: A description of observations and ideas with focus on the period prior to the International Polar Year 2007–2009. *Progress in Oceanography*, *132*, 22–67. https://doi.org/10.1016/j.pocean.2013.11.006

Rudels, B., Jones, E. P., Schauer, U., & Eriksson, P. (2004). Atlantic sources of the Arctic Ocean surface and halocline waters. *Polar Research*, *23*(2), 181–208. https://doi.org/10.3402/polar.v23i2.6278

Rysgaard, S., Glud, R., Sejr, M., Bendtsen, J., & Christensen, P. (2007). Inorganic carbon transport during sea ice growth and decay: A carbon pump in polar seas. *Journal of Geophysical Research: Oceans*, *112*(C3). https://doi.org/10.1029/2006jc003572

Saito, M. A., Moffett, J. W., & DiTullio, G. R. (2004). Cobalt and nickel in the Peru upwelling region: A major flux of labile cobalt utilized as a micronutrient. *Global Biogeochemical Cycles*, *18*(4). https://doi.org/10.1029/2003gb002216

Sakshaug, E. (2004). Primary and secondary production in the Arctic Seas. In *The organic carbon cycle in the Arctic Ocean*, (pp. 57–81). Springer. https://doi.org/10.1007/978-3-642-18912-8_3

Schauer, U., Rudels, B., Jones, E. P., Anderson, L. G., Muench, R. D., Björk, G., et al. (2002). *Confluence and redistribution of Atlantic water in the Nansen, Amundsen, and Makarov basins, Annales Geophysicae*, 20, 257–273, https://doi.org/10.5194/angeo-20-257-2002

Schlitzer, R., Anderson, R. F., Dodas, E. M., Lohan, M., Geibert, W., Tagliabue, A., et al. (2018). The GEOTRACES intermediate data product 2017. *Chemical Geology*, *493*, 210–223.

Schlosser, P., Kromer, B., Östlund, G., Ekwurzel, B., Bönisch, G., Loosli, H., & Purtschert, R. (1994). On the ^{14}C and ^{39}Ar distribution in the central Arctic Ocean: Implications for deep water formation. *Radiocarbon*, *36*(3), 327–343. https://doi.org/10.1017/s003382220001451x

Sclater, F., Boyle, E., & Edmond, J. (1976). On the marine geochemistry of nickel. *Earth and Planetary Science Letters*, *31*(1), 119–128. https://doi.org/10.1016/0012-821x(76)90103-5

Sherrell, R. M., & Boyle, E. A. (1992). The trace metal composition of suspended particles in the oceanic water column near Bermuda. *Earth and Planetary Science Letters*, *111*(1), 155–174. https://doi.org/10.1016/0012-821x(92)90176-v

Shimada, K., Itoh, M., Nishino, S., McLaughlin, F., Carmack, E., & Proshutinsky, A. (2005). Halocline structure in the Canada Basin of the Arctic Ocean. *Geophysical Research Letters*, *32*(3). https://doi.org/10.1029/2004gl021358

Slagter, H. A., Laglera, L. M., Sukekava, C., & Gerringa, L. J. A. (2019). Fe-binding organic ligands in the humic-rich Transpolar Drift in the surface Arctic Ocean using multiple voltammetric methods. *Journal of Geophysical Research: Oceans*, *124*(3), 1491–1508. https://doi.org/10.1029/2018jc014576

Slagter, H. A., Reader, H. E., Rijkenberg, M. J. A., van der Rutgers Loeff, M., de Baar, H. J. W., & Gerringa, L. J. A. (2017). Organic Fe speciation in the Eurasian Basins of the Arctic Ocean and its relation to terrestrial DOM. *Marine Chemistry*, *197*, 11–25. https://doi.org/10.1016/j.marchem.2017.10.005

Spivack, A. J., Huested, S. S., & Boyle, E. A. (1983). Copper, nickel, and cadmium in the surface waters of the Mediterranean. In C. S. Wong, E. Boyle, K. W. Bruland, J. D. Burton, & E. D. Goldberg (Eds.), *Trace metals in sea water* (pp. 505–512). Boston, MA: Springer US. https://doi.org/10.1007/978-1-4757-6864-0_30

Steele, M., Morison, J., Ermold, W., Rigor, I., Ortmeyer, M., & Shimada, K. (2004). Circulation of summer Pacific halocline water in the Arctic Ocean. *Journal of Geophysical Research: Oceans*, *109*(C2). https://doi.org/10.1029/2003jc002009

Sunda, W. G. (2012). Feedback interactions between trace metal nutrients and phytoplankton in the ocean. *Frontiers in Microbiology*, *3*. https://doi.org/10.3389/fmicb.2012.00204

Talley, L. D., Pickard, G. L., Emery, W. J., & Swift, J. H. (2011). Chapter 12—Arctic Ocean and Nordic Seas. In *Descriptive physical oceanography* (6th ed., edited, pp. 401–436). Boston: Academic Press. https://doi.org/10.1016/b978-0-7506-4552-2.10012-5

Tanhua, T., Jones, E. P., Jeansson, E., Jutterström, S., Smethie, W. M., Wallace, D. W. R., & Anderson, L. G. (2009). Ventilation of the Arctic Ocean: Mean ages and inventories of anthropogenic CO_2 and CFC-11. *Journal of Geophysical Research: Oceans*, *114*(C1), C01002. https://doi.org/10.1029/2008jc004868

Taylor, R. L., Semeniuk, D. M., Payne, C. D., Zhou, J., Tremblay, J. É., Cullen, J. T., & Maldonado, M. T. (2013). Colimitation by light, nitrate, and iron in the Beaufort Sea in late summer. *Journal of Geophysical Research: Oceans*, *118*(7), 3260–3277. https://doi.org/10.1002/jgrc.20244

Timmermans, M.-L., Garrett, C., & Carmack, E. (2003). The thermohaline structure and evolution of the deep waters in the Canada Basin. *Arctic Ocean, Deep Sea Research Part I: Oceanographic Research Papers*, *50*(10), 1305–1321. https://doi.org/10.1016/s0967-0637(03)00125-0

Tovar-Sánchez, A., Duarte, C. M., Alonso, J. C., Lacorte, S., Tauler, R., & Galbán-Malagón, C. (2010). Impacts of metals and nutrients released from melting multiyear Arctic sea ice. *Journal of Geophysical Research: Oceans*, *115*(C7), C07003.

Twining, B. S., & Baines, S. B. (2013). The trace metal composition of marine phytoplankton. *Annual Review of Marine Science*, *5*, 191–215. https://doi.org/10.1146/annurev-marine-121211-172322

Twining, B. S., Baines, S. B., Vogt, S., & Nelson, D. M. (2012). Role of diatoms in nickel biogeochemistry in the ocean. *Global Biogeochemical Cycles*, *26*(4). https://doi.org/10.1029/2011gb004233

Vieira, L. H., Achterberg, E. P., Scholten, J., Beck, A. J., Liebetrau, V., Mills, M. M., & Arrigo, K. R. (2019). Benthic fluxes of trace metals in the Chukchi Sea and their transport into the Arctic Ocean. *Marine Chemistry*, *208*, 43–55. https://doi.org/10.1016/j.marchem.2018.11.001

Vraspir, J. M., & Butler, A. (2009). *Chemistry of marine ligands and siderophores*.

Westerlund, S. F. G., Anderson, L. G., Hall, P. O. J., Iverfeldt, Å., Van Der Loeff, M. M. R., & Sundby, B. (1986). Benthic fluxes of cadmium, copper, nickel, zinc, and lead in the coastal environment. *Geochimica et Cosmochimica Acta*, *50*(6), 1289–1296. https://doi.org/10.1016/0016-7037(86)90412-6

Whitby, H., & van den Berg, C. M. (2015). Evidence for copper-binding humic substances in seawater. *Marine Chemistry*, *173*, 282–290. https://doi.org/10.1016/j.marchem.2014.09.011

Wood, P. M. (1978). Interchangeable copper and iron proteins in algal photosynthesis: Studies on plastocyanin and cytochrome c-552 in *Chlamydomonas*. *European Journal of Biochemistry*, *87*(1), 9–19. https://doi.org/10.1111/j.1432-1033.1978.tb12346.x

Woodgate, R. A., Aagaard, K., Muench, R. D., Gunn, J., Björk, G., Rudels, B., et al. (2001). The Arctic Ocean boundary current along the Eurasian slope and the adjacent Lomonosov Ridge: Water mass properties, transports, and transformations from moored instruments. *Deep Sea Research Part I: Oceanographic Research Papers*, *48*(8), 1757–1792. https://doi.org/10.1016/s0967-0637(00)00091-1

Woodgate, R. A., Aagaard, K., Swift, J. H., Falkner, K. K., & Smethie, W. M. (2005). Pacific ventilation of the Arctic Ocean's lower halocline by upwelling and diapycnal mixing over the continental margin. *Geophysical Research Letters*, *32*(18). https://doi.org/10.1029/2005gl023999

Xiang, Y., & Lam, P. J. (2020). Size-fractionated compositions of marine suspended particles in the Western Arctic Ocean: Lateral and vertical sources. *Journal of Geophysical Research: Oceans*, *125*(8), e2020JC016144.

Yamamoto-Kawai, M., McLaughlin, F., Carmack, E., Nishino, S., & Shimada, K. (2008). Freshwater budget of the Canada Basin, Arctic Ocean, from salinity, $\delta^{18}O$, and nutrients. *Journal of Geophysical Research: Oceans*, *113*(C1).

Yamamoto-Kawai, M., McLaughlin, F., Carmack, E., Nishino, S., Shimada, K., & Kurita, N. (2009). Surface freshening of the Canada Basin, 2003–2007: River runoff vs. sea ice meltwater. *Journal of Geophysical Research: Oceans*, *114*(C1).

Yeats, P. A. (1988). Manganese, nickel, zinc, and cadmium distributions at the Fram-3 and Cesar ice camps in the Arctic Ocean. *Oceanologica Acta*, *11*(4), 383–388.

Yeats, P. A., & Westerlund, S. (1991). Trace metal distributions at an Arctic Ocean ice island. *Marine Chemistry*, *33*(3), 261–277. https://doi.org/10.1016/0304-4203(91)90071-4

Yeats, P. A., Westerlund, S., & Flegal, A. R. (1995). Cadmium, copper, and nickel distributions at four stations in the eastern central and south Atlantic. *Marine Chemistry*, *49*(4), 283–293. https://doi.org/10.1016/0304-4203(95)00018-m

Zhang, R., Jensen, L. T., Fitzsimmons, J. N., Sherrell, R. M., & John, S. (2019). Dissolved cadmium and cadmium stable isotopes in the Western Arctic Ocean. *Geochimica et Cosmochimica Acta*, *258*, 258–273. https://doi.org/10.1016/j.gca.2019.05.028